Chair of Reservoir Engineering

Master's Thesis

Emulsions and Wettability Observations in Powdered Rock

Christian Wimmer, BSc

October 2019

To my beloved parents and brothers.

EIDESSTATTLICHE ERKLÄRUNG

Ich erkläre an Eides statt, dass ich diese Arbeit selbständig verfasst, andere als die angegebenen Quellen und Hilfsmittel nicht benutzt, und mich auch sonst keiner unerlaubten Hilfsmittel bedient habe.

Ich erkläre, dass ich die Richtlinien des Senats der Montanuniversität Leoben zu "Gute wissenschaftliche Praxis" gelesen, verstanden und befolgt habe.

Weiters erkläre ich, dass die elektronische und gedruckte Version der eingereichten wissenschaftlichen Abschlussarbeit formal und inhaltlich identisch sind.

Datum 01.10.2019

Unterschrift Verfasser/in
Christian, Wimmer
Matrikelnummer: 01335118

Acknowledgements

I want to thank Prof. Holger Ott, for his supervision during the creation of this thesis and for his guidance during my stay abroad. I also want to thank Dr. Thomas Finkbeiner and Prof. Santamarina for their supervision and the whole ANPERC team at KAUST for their help and support.

This work would not have been possible without my family, who helped me during my studies by being always there for me when I needed something.

Thank you also to all my friends at Montanuniversität Leoben, especially my former roommates. You made life more enjoyable through all those years and are therefore part of my academic success.

Abstract

Designing EOR methods like low salinity waterflooding, requires an accurate assessment of the wettability of the oil-water-reservoir rock system and a vast understanding of the mechanisms that define this property. Wettability tests by optical contact angle measurement on the rock surface or as a function of displacement properties within an intact core are common, but undamaged cores can be hard to retrieve. The possibility of determining the wettability from sedimentation tests of fine powder gathered by crushing rocks, is examined experimentally. Crushed Eagle Ford Rock, Bentonite, Illite, Kaolinite and Silica Flour are rained on polar and non-polar liquid interfaces and their residence time is recorded on video and analyzed in Matlab. Varying the salinity and the pH-value of the brine and the chemical composition of the hydrocarbon phase influences the residence time of the particles at the interfaces.

Pickering emulsions are investigated in theory and experimentally. Although surfactant-based emulsions are the industry standard in many EOR applications, the interest in nanoparticles serving as emulsifiers increased recently, due to their simplicity and resistance to coalescence. In a series of tests, they are formed by shaking vials containing the same particles used in the sedimentation tests. The observed emulsion type depends on the wettability of the particle. Water-wet particles form oil-in-water emulsions. Conversely, oil-wet particles form emulsions consisting of water droplets in oil. The droplet size of the dispersed phase and the stability of the emulsion is influenced by the salinity of the brine.

The sedimentation and emulsion tests are complemented by a series of imbibition tests, in which water imbibes kerosene-saturated pastes of different particles. The associated capillary forces cause fines migration and compaction leaving behind desiccation cracks. Imbibition and desiccation crack highlight water-preference, in other words water-wet mineral surfaces.

Keywords:

Wettability, EOR, Pickering emulsion, imbibition, desiccation crack

Zusammenfassung

Um tertiäre Ölgewinnungsmethoden, wie zum Beispiel die Injektion von Sole mit niedrigem Salzgehalt, zu optimieren, ist es nötig die Benetzung von Lagerstättengestein durch Öl und Wasser zu eruieren und die dahinterliegenden Mechanismen zu verstehen. Verschiedene Testmethoden, wie zum Beispiel die optische Bestimmung des Kontaktwinkels der Flüssigkeiten auf der Gesteinsoberfläche oder das Verhältnis von spontanem und erzwungenem Eindringen von Öl und Wasser in Lagerstättengestein ist üblich, aber intakte Bohrkerne können schwer zu bergen sein. Die Möglichkeit die Benetzung des Gesteins in Pulverform zu bestimmen, wird experimentell mittels Sedimentationstests untersucht. Das Regnen von pulverisiertem Eagle Ford-Gestein, Bentonit, Illit, Kaolinit und Kieselerde auf polare und unpolare Flüssigkeitsgrenzflächen, als Video aufgenommen und in Matlab analysiert, offenbart verschiedene Verweilzeiten der Partikel an der Grenzfläche. Diese kann durch Variation der Salinität oder des pH-Wertes der Sole oder durch das Verwenden von Kohlenwasserstoffen mit unterschiedlicher chemischer Zusammensetzung beeinflusst werden.

Pickering-Emulsionen werden im zweiten Teil der Arbeit theoretisch und experimentell untersucht. Obwohl auf Tensiden basierende Emulsionen als Industriestandard bei gewissen Anwendungen in der tertiären Ölgewinnung gelten, ist das Interesse an Nanopartikeln, die als Emulgatoren fungieren, in den letzten Jahren gestiegen. Dies liegt am einfachen Aufbau und dem exzellenten Widerstand gegen Koaleszenz. In der durchgeführten Testreihe werden dieselben Fläschchen, die schon in den Sedimentationstests verwendet werden, geschüttelt und anschließend untersucht. Es zeigt sich, dass der Typ der Emulsion von den Benetzungseigenschaften des Partikels abhängt. Bevorzugt dieses Wasser, entsteht eine Emulsion von Öltröpfchen in Wasser. Bei Ölaffinität des Teilchens ist es dementsprechend umgekehrt. Die Tröpfchengröße und die Stabilität der Emulsion hängt in beiden Fällen mit der Salinität der verwendeten Sole zusammen.

Die Sedimentations- und Emulsionstests werden von einer dritten Testreihe komplettiert, in der das spontane Eindringen von Wasser in verschiedene kerosingesättigte Pasten aus unterschiedlichen Gesteinspulvern untersucht wird. Die vorhandenen Kapillarkräfte führen zu Partikelmigration sowie -verdichtung und in weiterer Folge zu Trocknungsrissen. Spontanes Eindringen von Wasser und die Trocknungsrisse betonen die Wasseraffinität der jeweiligen Minerale.

Table of Contents

List of Figures

List of Tables

Nomenclature

A	area	[m²]
B	Bond number / Eötvös number	
c	ionic concentration	mol/L
F	force	[N]
F	Faraday's constant	$F = 9.648 \cdot 10^4$ C/mol
g	gravity	[m/s²]
G	free energy	[J/(K mol)]
H	curvature	[m⁻¹]
m	mass	[kg]
N_{av}	Avogadro's number	$N_{av} = 6.022 \cdot 10^{23}$ [1/mol]
P	pressure	[Pa] = [N/m²]
r	radius	[m]
R	gas constant	$R = 8.314$ J/(K mol)
T	temperature	[°C], [K]
u	settling speed	[m/s]
V	volume	[m³]
W	work	[J]
z	Ionic valence	[ ]
ε_0	permittivity of free space	$\varepsilon_0 = 8.85 \cdot 10^{-12}$ F/m
ζ	Zeta potential	[V]
ϑ	Debye-Hückel length	[m]
ρ	density	[kg/m³]
θ	contact angle	[°]
κ'	relative permittivity	[ ]
γ	interfacial tension/energy	[N/m] = [J/m²]
Π	disjoining pressure	[Pa] = [N/m²]
Φ_c	angle of vertical position of a particle	[°]
Ψ	contact angle with reference to horizon	[°]

Abbreviations

IEP   Isoelectric Point

Chapter 1

Introduction

The experimental section of this master thesis was done at the King Abdullah University of Science and Technology in Saudi Arabia within the framework of the Visiting Student Research Program (VSRP). During my stay of five months I was part of the Saudi Aramco research team of Carlos Santamarina, who leads the Energy GeoEngineering Research group (EGEL) at the Ali I. Al-Naimi Petroleum Engineering Research Center (ANPERC). My supervisor was Dr. Thomas Finkbeiner, who is Senior Research Scientist at ANPERC.

The original topic of the program offered by KAUST, was called "Hydrodynamical Behavior of Naturally Fractured Shale." The purpose of the study was to use the vast understanding of flow behavior in fractures of conventional reservoir rock depending on factors such as varying stresses, shearing, salinity precipitations and so on, within the research group and extend it to the less understood shale rocks.

A main component of the experimental setup would have been a normal load rig, similar to those described by other authors but without the shear stress component(Gutierrez, Øino et al. 2000, Cuss, Milodowski et al. 2011). The goal was to measure fracture permeability as a function of the normal load applied by an oedometer for different kinds of fluids. The intention was to use water, brine, an alcohol and kerosene as test fluids within the fracture of an Eagle Ford core in different sequences and concentrations to get a better understanding of the rock-fluid interactions. In particular, the influence of clay swelling on the decrease of permeability was to be demonstrated.

In preliminary tests, the hardness of multiple rock specimens from the same Eagle Ford rock has been determined using micro indenter tests. The specimens were then exposed to the four fluid types mentioned earlier and the change in hardness has been tracked by repeating the hardness tests every 24 hours for a few days.

The Eagle Ford rock available was extremely hydrophobic and the water-based test fluids did not imbibe into the matrix in reasonable amounts. On the contrary, kerosene entered the rock matrix quite readily and seemingly dissolved organic components within the rock, which was evident because of the change in color from basically transparent to a slight yellow.

While the results of the hardness tests are quite interesting, the imbibition of the kerosene and the failure of the other fluids to do so, put the main experiment into question. After all, the hydrocarbons would saturate the rock matrix, while the water-based fluids that are causing clay swelling would not penetrate the matrix, as demonstrated during the hardness tests.

To evaluate how to circumvent this issue, tests on Eagle Ford rock powder have been conducted. The idea was to increase surface area and speed up possible interaction between the rock and water. However, the hydrophobic behavior remained evident as the fine powder would just sit on top of the water surface without sinking and even withstanding attempts to push it under water or steer it properly. During extensive literature research with the purpose to overcome the difficulties, I discovered a paper convincing enough to overhaul the whole project (Dubey and Doe 1993). In consultation with all involved supervisor, we decided to focus more on the fundamentals of rock-fluid interactions instead of fracture flow behavior.

Simple experiments with powdered Eagle Ford rock, three kinds of clay minerals and silica flour and their interaction with water, brine and kerosene would provide the basis for the three test-series described in this master thesis. A literature review on selected topics of wettability and minerology completes the final intention of the thesis, namely, to increase the understanding on basic principles of particle-fluid interactions.

1.1   Organization

Chapter 2 explores wettability, starting with basic concepts of the interfacial tension and capillarity. The commonly used Young-Laplace equation is expanded by the disjoining pressure to incorporate the concept of a thin layer. In Chapter 3 clay mineralogy, hydration of particles, the formation of a double layer and other interparticle forces are analyzed and related to the wettability. Chapter 4, 5 and 6 describe the experiments of the sedimentation, emulsion and imbibition test respectively. The former test series is used to demonstrate the influence of wettability on a particle at a liquid interface experimentally. A physical explanation given by a force analysis and an energy analysis links the wettability of a particle to its vertical position at the interface affecting its affinity to surpass the interface or form different types of emulsions, which is topic of Chapter 5. The emulsion test in Chapter 6 uses the same concept of particle-fluid interaction and demonstrates directly the influence of wettability on spontaneous imbibition.

Chapter 2

Concept of Wetting

Wetting is an umbrella term, used to describe interfacial behavior at intersections of three phases of which at least two are fluids. It describes the tendency of a solid to either spread water or to form isolated droplets on its surface and is of great significance in everyday situations. Raincoats consist of coated fiber with water-repealing characteristics, just like water does not penetrate feathers of a duck allowing it to stay warm and to float on water. This behavior is called hydrophobic and contrary to surfaces encountering water that spreads on its surface which is called hydrophilic. These two terms are specifically used to describe the affinity for a surface for water and can be replaced by more general terms of lyophilicity and lyophobicity (Lyklema 2005).

The interfacial behavior of different phases at an interface depends on the interfacial tension between those phases. Interfacial tension can be illustrated both as a free energy per unit area and as a force per unit length. The moveable part of a wire frame enclosing a soap film shown in Fig. 1 can be moved to the right by investing work according to:

$$dW = \gamma l\, dx = \gamma\, dA \tag{1}$$

where dW is the work required to extend the moveable part of the frame by a distance dx against the force per unit length γ. This is equivalent to a free energy per unit area using the same notation γ multiplied with the change in area A. While both parts of the equation are equivalent, they represent two different concepts used in interfacial science. Whether surface tension with the unit N/m or surface free energy in J/m^2 is used, remains a choice of personal preference. Depending on the topic both approaches are used in this thesis. (Adamson and Gast 1967)
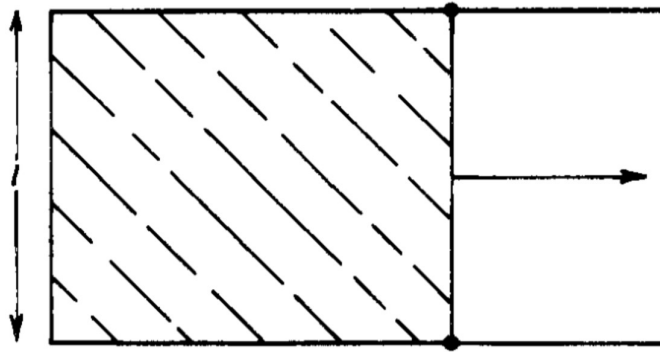
Figure 1: A wire frame enclosing a soap film, showing the concept of interfacial tension (Adamson and Gast 1967)

The theory behind capillarity (Young 1855) and its mathematical principle (de Laplace 1807) led to the equation that was later called the Young-Laplace equation:

$$\Delta P = \gamma \left(\frac{1}{R_1} + \frac{1}{R_2} \right) \tag{2}$$

where ΔP is the pressure difference across the fluid interface, γ is the surface free energy and $R_{1,2}$ are the radii of curvature. It is the fundamental equation of capillarity and one of the central equations of this chapter.

For spherical shaped interfaces R_1 and R_2 are equal, therefore Eq. (2) can be reduced to:

$$\Delta P = \frac{2\gamma}{R} \tag{3}$$

For plane surfaces mathematically described by an infinite radius, the pressure difference is zero (Adamson and Gast 1967).

A simple thought experiment to illustrate wetting and its definitions, consists of a droplet of water on a flat surface in an air environment (see Fig. 2). Here, three different phases are present, namely water, air and the solid surface.
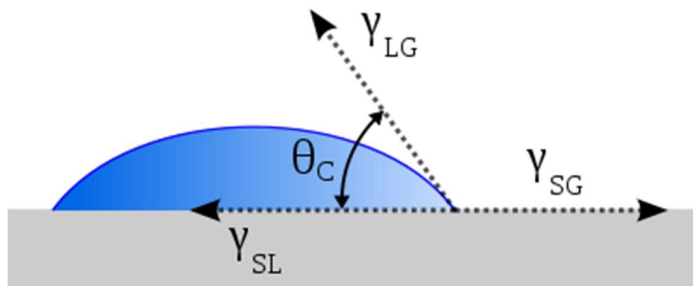
Figure 2: Young's law of the contact angle (source: Wikipedia.org)

The shape of the droplet depends on the tensions that apply on the interfaces between the three media. If analyzed in the two-dimensional cross section, the three distinct phases intersect in a point at the edge of the droplet. At this point, the three interfacial tensions

- γ_{SL} … Interfacial tension between the solid surface and the droplet of liquid
- γ_{SG} … Interfacial tension between the solid surface and the gas phase (air in this case)
- γ_{LG} … Interfacial tension between the droplet of liquid and the gas phase

can be described by Young's law:

$$\gamma_{SG} - \gamma_{SL} = \gamma_{LG} \cdot \cos \theta_C \tag{4}$$

The angle of the droplet at the intersection point is a function of the three interfacial tensions. The angle is usually measured through the denser medium. the liquid phase in a gas-liquid-solid system. In a liquid-liquid-solid system, an indication of the liquid through which the angle is measured, should be given.

2.1 Thermodynamics of Wetting on a microscopic Scale

Surface and interfacial tensions refer to macroscopic amounts of fluid and can be analyzed by thermodynamic approaches. On a colloidal and molecular scales, this approach needs to be complimented by statistical thermodynamics based on assumptions on interactions between molecules. Van der Waals forces explain monomolecular layers of water molecules on hydrophobic surfaces and why water droplets attach to hydrophobic surfaces in a gas environment. Detachment of same droplet only happens, if water-water attraction (sometimes referred to as cohesion) outweighs the water-solid attraction (adhesion).
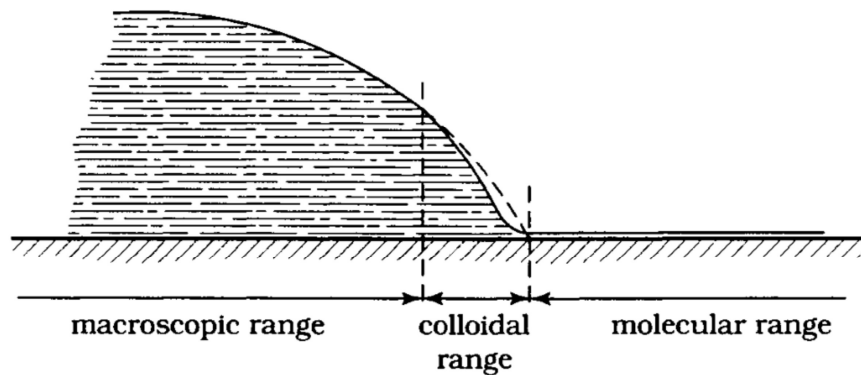
Figure 3: Different ranges apply in the thermodynamic relationship of wetting (Lyklema 2005)

The different ranges discussed above are illustrated in Figure 3. The macroscopic range (10^2 nm and above) and the molecular range (1nm and below) is separated by a transition zone called colloidal range. The dashed line within the transition zone represents the edge of the droplet without considering intermolecular forces. Experimental methods using microscope

interference techniques however have provided evidence for a curvature influenced by intermolecular forces (Kolarov, Zorin et al. 1990).

The meniscus of a liquid on a solid surface can be observed with the naked eye. It is the macroscopic relationship of interfacial tensions and the enclosed contact angle described by Young's law in Eq 4 However, as indicated in Fig. 3, at smaller ranges the fluid at the intersection of the three phases is different and does not follow Young's law. Monolayers or very thin layers have been proposed to separate the fluid that shows less tendency for wetting of the solid surface (Dubey, 1993). The thickness of this layer is a thermodynamic variable defined by the disjoining pressure, or expressed as a force, is the force that tends to separate the two interfaces.

To describe the thermodynamic equilibrium of the flat fluid layer, Young's law in its simple form has to be extended by adding the disjoining pressure or force per unit area term Π (Hirasaki 1991). For simplicity, the radii of curvature are substituted by H, which is the mean curvature.

$$\Delta P = \Pi + 2H\gamma \tag{5}$$

Eq. 5 is visualized in Fig. 4.
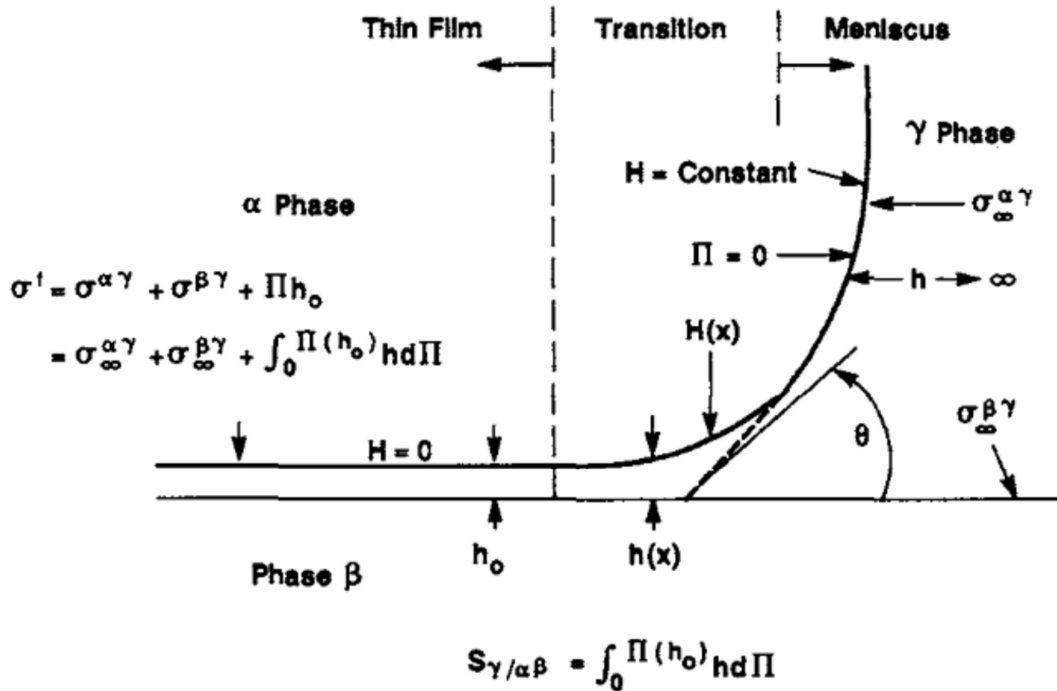
Figure 4: Intersection of two fluids and a solid surface on a molecular scale

The curvature in the thin section is zero hence the second term in Eq. 5 is zero and the capillary pressure ΔP only depends on the disjoining pressure Π. In the meniscus area, the curvature is

non-zero while the disjoining pressure becomes infinitesimal because of the relatively high height difference between the layers compared to the thin section.

According to the principle of free energy, a thermodynamic system tries to minimize its free energy to reach an equilibrium. The system in Fig. 4 is in equilibrium, therefore the height of thin film and the disjoining pressure can be called the equilibrium height h_{eq} and the corresponding disjoining pressure Π_{eq} respectively. The latter can be calculated by changing Eq. 5 to

$$\Pi_{eq} = \Delta P - 2H\gamma \tag{6}$$

To change the film thickness, work must be applied leading to a change in potential energy:

$$\Delta\omega = \int_{h}^{h_{eq}} \left[\Pi(h') - \Pi_{eq}\right] dh' \tag{7}$$

Here $\Delta\omega$ is the change in potential per unit area and $\Pi(h')$ is the disjoining pressure at the investigated height h'. If the height changes from the equilibrium height, the potential energy is changed too. The complex interactions of electrostatic and molecular forces relevant for the so-called DLVO theory (described in Chapter 3.4) can lead to multiple metastable configurations of the thermodynamic system and therefore multiple stable thicknesses.

2.2 Hysteresis of the Contact Angle

The dynamic contact angle of moving droplets on solid surfaces is a function of the velocity of movement, which has been proved experimentally by tensiometric methods (Hayes, Ralston et al. 1993). Advancing contact angles (angle between liquid surface and solid substrate at the contact line of the droplet that moves towards previously unwetted solid surface) increase with speed, in contrast to receding contact angles which decrease with speed. Fig. 5 shows the contact angle as a function of velocity and indicates a step at a velocity equal to zero demonstrating that at static conditions contact angle changes caused by a change in external forces without accelerating the droplet.

The difference in static advancing and receding angle leads to a hysteresis function, that makes static, optical measurement of the contact angle difficult. The size of the hysteresis is influenced by the geometry and on the wettability of the contacted areas on the substrate if non-homogeneous.
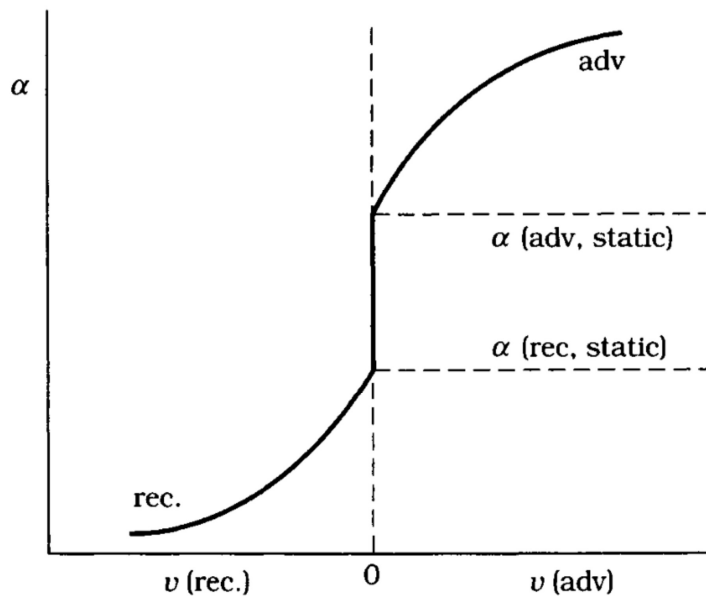
Figure 5: Contact angle as a function of the water droplet velocity (Lyklema 2005)

2.3 Wettability in Petroleum Engineering

Wettability has been identified as a major factor in many aspects of Petroleum Engineering, controlling all types of core analysis and assessments using capillary pressures and relative permeability (Anderson 1986). Wettability is decisive in multi-phase flow problems that occur during various stages of the lifecycle of a reservoir. During the migration of hydrocarbons from the source rock to the reservoir rock, the chemical composition of the crude and the mineral composition of the reservoir rock influence among other factors the distribution and accessibility of the hydrocarbons within the reservoir. During the drilling period it is desirable

to keep imbibition of mud into the reservoir matrix small to mitigate fluid loss and prevent formation damage. Wettability and consequently capillary pressure are factors that control this process. However, the most important area of application for the concept of wettability is Reservoir Engineering, especially in Enhanced Oil Recovery, where the goal is to increase the recovery factor of reservoirs to increase profitability and lifetime of wells.

Generally, the contact angle is measured within the denser medium. In Petroleum Engineering related topics which are usually dealing with oil and water as the liquid phases, the latter is therefore the phase through which the contact angle is measured. Reservoir rock wettability is described by the strongest affinity for either water or oil, hence systems with contact angles smaller than 90° are called water wet.

Contact angle [°]	
0	Complete water wet system
<90°	Water wet
90°	Intermediate or neutral wet
>90°	Oil wet system

At this point it has to be noted that in Petroleum Engineering related wettability measurements, for example on retrieved cores or plugs, rarely deals with flat surfaces, but with porous rocks instead. Optical measurements of contact angles are difficult, but qualitative assumptions can be made by comparing the behavior of oil and water in displacement tests. The rock has a higher affinity for the fluid that spontaneously imbibes into the rock.

2.3.1 Wettability Measurements

Reservoir wettability is not a physical property that can be exactly measured and compared. Instead it is a general tendency of the flow behavior of two or more fluids within the pores of a reservoir rock. Different methods developed over the years often measure different physical properties that are often not easily comparable. Adhesion test (see Appendix 7.3 for more details) measure macroscopic contact angles of droplets on various surfaces, but are difficult to relate to the reservoir rock. Surface contaminations, heterogeneities, roughness and other interface properties can complicate measurements and make the acquisition of reproducible results difficult (Morrow 1990).

The porous structure and its influence on wettability is better shown in Amott and USBM tests (see Appendix 7.3.2 and 7.3.3), but those experiments ideally need an intact core close to reservoir conditions which is hard to acquire.

Wettability can also be investigated not from intact rocks but from rock powders, which are easier to gather for example from cuttings. Film Flotation (Fuerstenau, Diao et al. 1991) is a method to get the critical wetting surface tension of particles by measuring the percentage of particles that float as a function of the surface tension of an aqueous methanol solution. The surface tensions are changed by changing the ratio of water and methanol in the solution. It is not only a method to measure wettability of solids but is also used for physical separation of different kinds of particles for example in the mining industry.

2.3.1.1   Base Number and Wetting Properties of Crude Oil

Additionally, useful qualitative measurements to classify wettability exist. The so called bottle test (Dubey and Doe 1993) estimates the pH threshold that determines whether crude oil attaches onto rock particles or not.

Electrostatic interactions define wetting behavior of oil and water towards a solid surface in a typical reservoir system. Measuring the zeta potential directly (see Chapter 3.4), gives insight into the surface charge of solid particles and the charge of the hydrocarbon phase and allows prediction of wetting behavior. Opposing surface charges of solids and the crude leads to electrostatic repulsion and favors water-wet behavior of the solid.
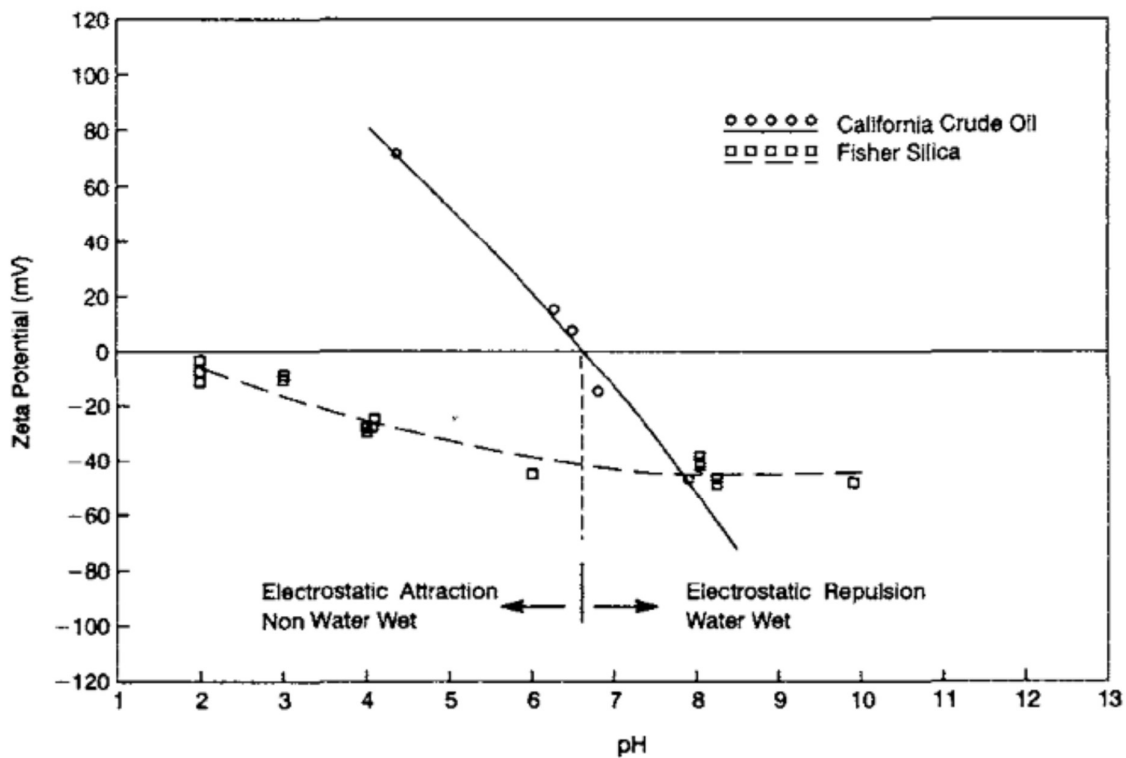
Figure 6: Zeta Potential of a crude and silica as a function of pH (Dubey and Doe 1993)

Fig. 6 shows the zeta potential of California crude and silica as a function of the pH. While pure hydrocarbons have a low zeta potential for low values of pH, crudes show high zeta potentials at similar regimes. The zeta potential of the silica surface is negative at all pH-values investigated, leading to electrostatic attraction in the lower pH-regime below 6.7. Above that range, surface charge of the crude turns negative and thus results in electrostatic repulson.

The bottle test is a simple test to determine the wetting behavior of fine silica in an oil-brine environment by observing the tendency of the particles to attach to either phase. Oil-wet behavior, in which the silica stays above the oil-brine interface is caused by electrostatic attraction between the opposite charges of silica and the hydrocarbon phase. However, if the silica sinks to the ground electrostatic repulsion between solid and crude indicates water wet behavior. The identification of the pH value at which electrostatic reversal happens is the result of the test.

2.3.2 Reservoir Wettability Alteration

When the significance of wettability as a reservoir property, that can significantly influence the recovery factor, became more important in the 70's and 80's of the last century, the general assumption was that reservoirs had to be initially strongly water wet. This assumption was based on the process of hydrocarbon migration in which oil or gas is migrating into reservoir formations displacing reservoir water. The reservoir rock was assumed to maintain its water-wet tendency affiliated with the formation water even after the introduction of hydrocarbons from migration. Today we know, wettability reversal can be achieved by a single layer of molecules on solid surface. Clean quartz, that is completely water wet, can be turned oil wet by coating it with a monolayer of polar molecules (Morrow 1990).

Especially high-molecular weight polar molecules have been proven to alternate wetting behavior of reservoir rocks. By comparing USBM wettability tests done on asphaltene treated Berea sandstones with the untreated counterparts, it has been proven that completely water wetting sandstones (USBM index = +0.97) can be turned intermediate wetting (USBM index = +0.12, Dubey and Waxman (1991)). Asphaltene removal by precipitation has been shown to make crude oils less adhesive (Buckley and Morrow (1990)).

Generally, in Reservoir Engineering water-wet reservoir rock is desired, because of the higher mobility of the crude. Numerous enhanced oil recovery methods that change wettability towards water-wet exist. A convenient and very often used method is low salinity water flooding to increase productivity of oil wells. By increasing electrostatic repulsion between heavy oil molecules and clay-containing reservoirs, the tendency of oil to attach to the rock is decreased. In other words, the reservoir rock is turning water-wet. In terms of the thermodynamics on a microscopic level discussed in Chapter 2.1, the equilibrium height of the

thin section which is water is increased. In terms of particle-fluid interaction (see Chapter 3.3), a decrease in salinity, increases the double layer size of colloidal particles, which for clays results in swelling. In the industry it is sometimes called controlled destruction of the reservoir rock, because a too low salinity lead to the disintegration of the rock.

Chapter 3

Particle-fluid Interactions and Fabric Formation

The purpose of this chapter is to provide a literature review on relevant fields of minerology and particle-fluid interactions and forces. Additionally, it analyzes why and how clay particle associations are influenced by changes in wettability, pH and salinity.

3.1 Mineralogy of Clay Minerals

Clay minerals or physio silicates are extensively investigated in the Petroleum industry. Many stuck pipe events in drilling are related to clay swelling, a process vastly observed in clay horizons rich in Bentonite. Other clay minerals are less prone to swelling due to a different mineral structure.

Clay minerals are composed of sheets of which at least one layer is a silica mineral. It is composed of tetrahedrons (Fig. 7 (a)) with Si^{4+} in the center of four O^{2-}. Additional components of clay minerals are Gibbsite sheets and Brucite sheets made up of octahedrons with Al^{3+} or Mg^{2+} in the center of octahedrons respectively with O^{2-} at their vertices (Fig. 7 (b)) (Santamarina, Klein et al. 2001).

	Si tetrahedron	Al or Mg octahedron
(a) Building components	center: Si^{4+} corners: O^{2-}	center: Al^{3+} (or Mg^{2+}) corners: OH^- (or O^{2-})
(b) Sheets	Si tetrahedral sheet: Silica	Al octahedral sheet: Gibbsite (G) Mg octahedral sheet: Brucite
(c) Unit layers	Kaolinite 1:1 — 7.2 Å	Illite (low swell) 2:1 — 10 Å	Montmorillonite (high swell) 2:1 — 10-20 Å water/cations
(d) Termination sites on particle faces and edges	1:1 minerals	2:1 minerals

Note: edge and face charge vary with pH

Figure 7: Mineral structure and building components of clay minerals

Kaolinite consists of units of a silica layer and one Gibbsite layer. Due to their distinct building components, the two sheets display dissimilar surface charges or so-called termination sites on the particle faces (see Fig. 7 (c) and (d)). The valence of the termination site influences the type and strength of the connection between the units. For Kaolinite the units are strongly held together by hydrogen bonding and therefore swelling is limited. Fig. 8 below shows a SEM image visualizing the platy, hexagonal structure of the Kaolinite mineral.
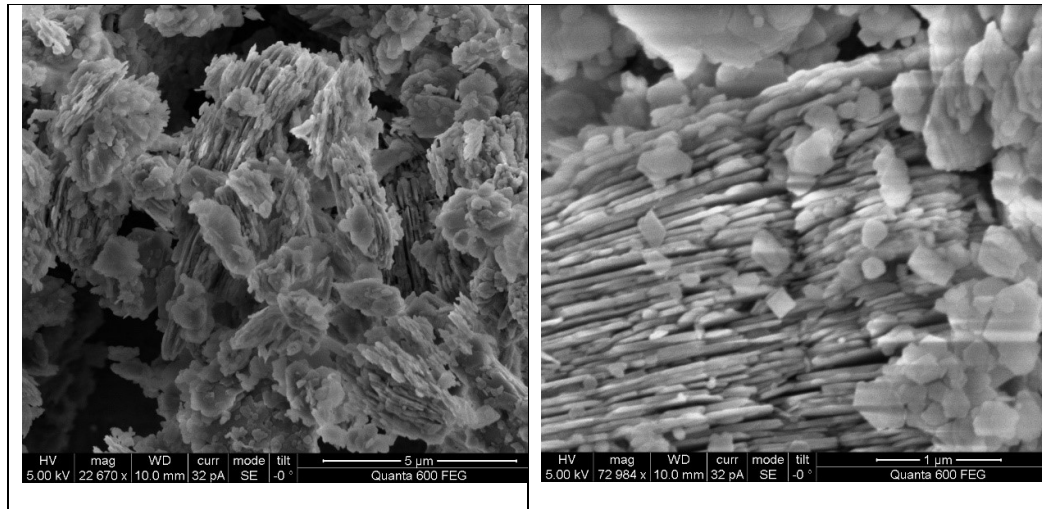
Figure 8: SEM-images of Kaolinite mineral structures

Illite units are made of two silica layers with a layer of Gibbsite in between. The silica layers on the outside restricts the type of the termination site on the face of the particle to O^{2-}. Potassium ions between the units make up the rest of Illite mineral and restrict swelling.

Montmorillonite minerals are prone to swelling. It has a unit structure similar to Illite (see Appendix 7.4), but instead of K^+ different kinds of ions and water molecules connect the units allowing swelling of the structure. Just like Illite, the free face of the particle consists of O^{2-}-termination sites.

3.2   Liquids

The interactions between solid particles and liquids influence all experiments discussed in this thesis. To predict the behavior of the solids at liquid interfaces or the stability of emulsion, one must understand the basic principles of the structure of the liquids used.

Water is a molecule made from one oxygen and two hydrogen atoms. The latter are oriented in an angle of 109° to satisfy the condition of minimum potential in the molecule leading to a special case of interaction between molecules called hydrogen bonding. In the near field it determines the packing of the water molecule in the bulk fluid and on surfaces. For distances higher than three radii, water molecules can be simplified as dipoles.

If salt is dissolved in water, they split into positively and negatively charged ions and are hydrated by water molecules, due to the polarity of the water molecules and thermal agitation. Free water and hydrated ions coexist in electrolytes.

If sodium chloride is dissolved (Fig. 9, (1)), the negatively charged oxygen atom of the water molecule attaches to the positively charged Na-ion. The positively part of dipolar water molecules attaches to the negatively charged Cl-ion (Fig. 9 (2)). Hydration shells around the

ions are formed (Fig. 9 (3)), which consist of four to five H_2O molecules for Na^+ and one to two molecules for Cl^- (Fig. 9 (4)).
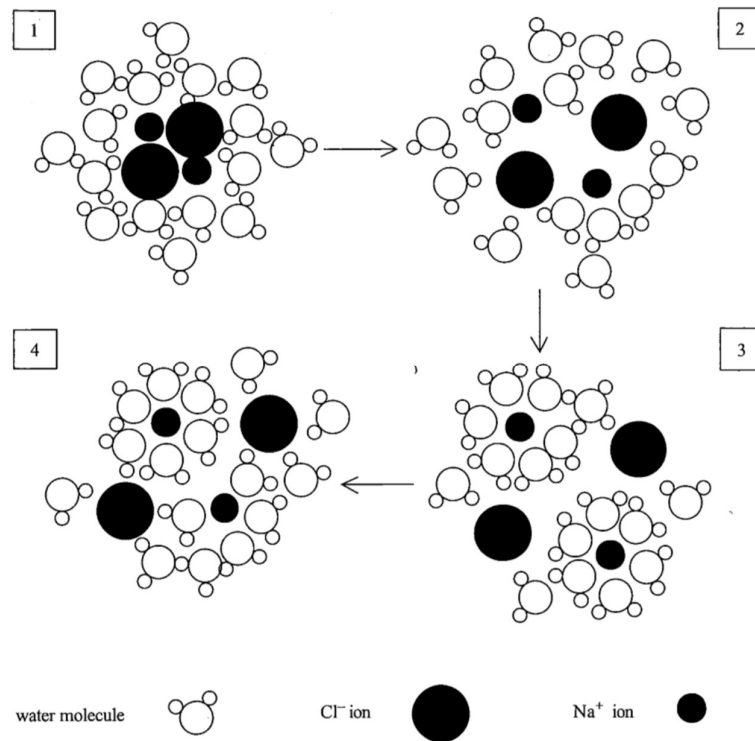
Figure 9: Hydration of sodium chloride (Santamarina, Klein et al. 2001)

The number of water molecules attaching to a single ion is called the Hydration number and depends on the size and the charge of the ion. The radius of Ca^{2+} for example is similar to Na^+, but has a hydration number of 6 ± 1, because of the higher charge compared to Na^+.

3.3   Particle-Fluid Interaction

Hydration is not restricted to ions in electrolytes, but also applies to charged surfaces or colloidal particles. Dry clay has a negative surface charge and adsorbs positive counterions and excess salt molecules without charge. After hydration, water dipoles attach to the adsorbed counterions and form so-called inner sphere complexes, partly hydrated with water molecules and attached to the surface, and outer sphere complexes, which are completely hydrated. The co and counter ions from the dissolved salt molecules are hydrated as well. Remaining water molecules acting as dipoles, rotate and align according to the charge of the solid surface. The degree of hydration of ions and the tendency of dipoles to align according to the surface charge increases with distance from the center of the clay particle, until it is similar to the bulk electrolyte at the edge of the so-called diffuse layer.
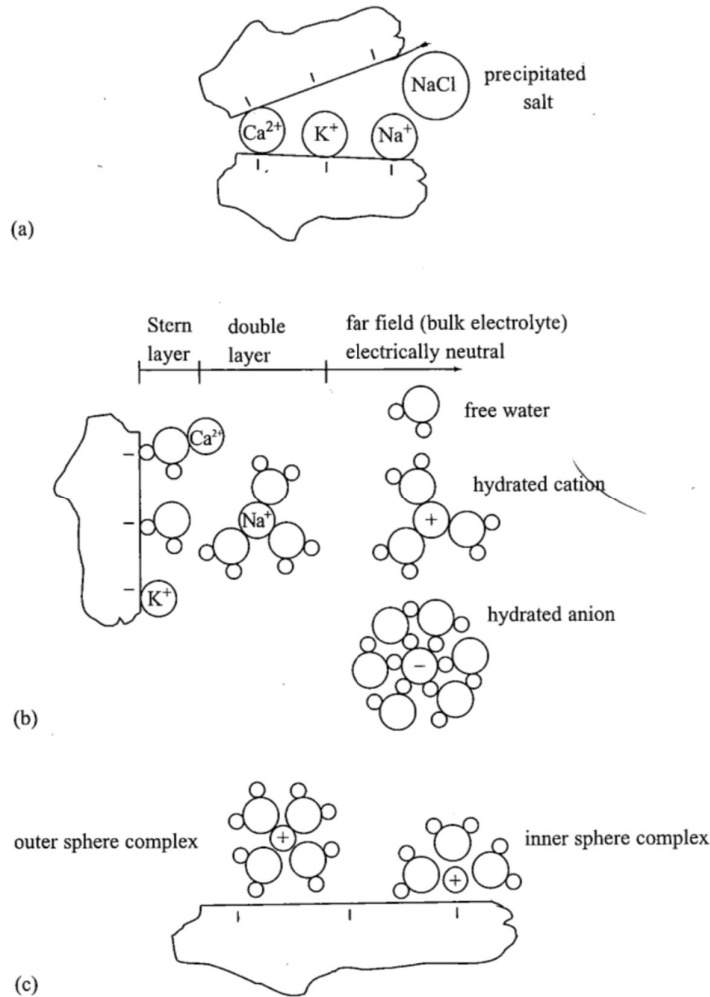
Figure 10: Dry clay (a), double layer structure on a clay surface (b) and structure of inner and out sphere complexes (c) (Santamarina, Klein et al. 2001)

The diffuse layer encloses the Stern layer, which characteristically has firmly attached counterions and inner sphere complexes (see Fig. 10). The interface of the two layers is called the outer Helmholtz plane and together the two layers make up the double layer of the solid particle.
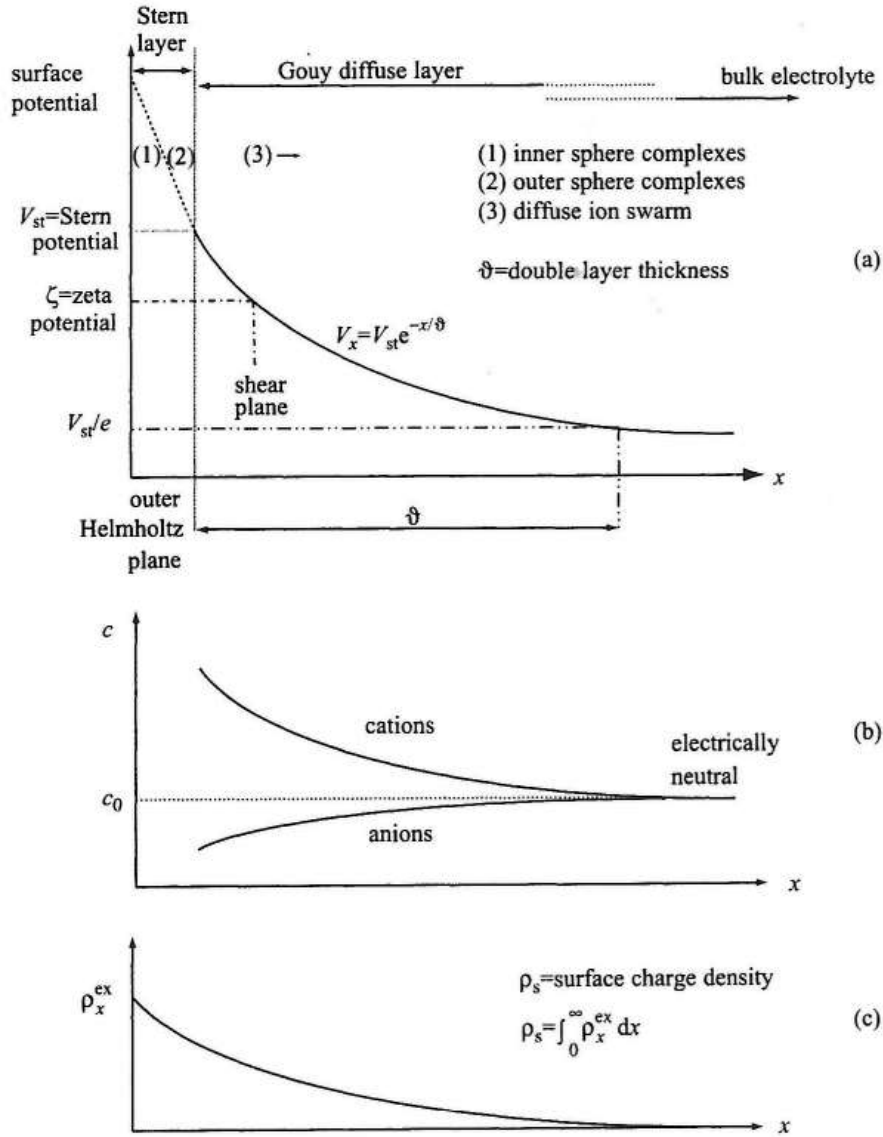
Figure 11: Double layer potential (a), concentration (b) and excess surface charge (c) (Santamarina, Klein et al. 2001)

The size of the double layer is difficult to fixate, as the transition from diffuse layer to bulk fluid is fuzzy. The Debye-Hückel length gives a reasonable size of the double layer and can be derived from Boltzmann's equation showing the ion distribution at equilibrium:

$$c_{ix} = c_0 \exp\left(\frac{-z_i F V_x}{RT}\right) \tag{8}$$

where c_{ix} is the ionic concentration of species i at a distance x from the particle in mol/m3, c_0 is the bulk fluid concentration (mol/L), z_i is the ionic valence, $F = 9.648 \cdot 10^4$ C/mol is Faraday's constant, V_x is the electrical potential at distance x from the surface (V), $R = 8.314$ J/(K mol) is the gas constant and T is absolute temperature.

Poisson's equation allows to calculate the distribution of excess charges ρ_x^{ex} within the double layer assuming electroneutrality, so that the integral of the excess charges is equal to the surface charge density:

$$\frac{\partial^2 V_x}{\partial x^2} = -\frac{\rho_x^{ex}}{\varepsilon_0 \kappa'} \tag{9}$$

where $\varepsilon_0 = 8.85 \cdot 10^{-12}$ F/m is the permittivity of free space and κ' is the relative permittivity of the fluid. The excess charge can be calculated from the valence and concentration:

$$\rho_x^{ex} = \sum_i z_i c_{ix} F \tag{10}$$

Combining Equ. 8, 9 and 10 yields:

$$\frac{\partial^2 V_x}{\partial x^2} = -\frac{c_0 F}{\varepsilon_0 \kappa'} \sum_i z_i \exp\left(\frac{-z_i F V_x}{RT}\right) \tag{11}$$

If the cations and anions have the same valence, Eq. 12 applies:

$$\frac{\partial^2 V_x}{\partial x^2} = -\frac{c_0 z F}{\varepsilon_0 \kappa'}\left[-\exp\left(\frac{-zF V_x}{RT}\right) + \exp\left(\frac{zF V_x}{RT}\right)\right] \tag{12}$$

Eq. 12 can be simplified for small surface potentials using the limit of $-e^{+y} + e^{-y}$ which is $2y$ for $y \to 0$.

$$\frac{\partial^2 V_x}{\partial x^2} = \frac{2c_0 z^2 F^2}{\varepsilon_0 \kappa' RT} V_x \tag{13}$$

The differential equation is solved for the boundary conditions of zero charge at infinite distance and fixed charge V_0 at the particle surface:

$$V_x \cong V_0 e^{-\frac{x}{\vartheta}} \tag{14}$$

Here ϑ is the Debye-Hückel length mentioned in the beginning. It is defined as the distance at which the potential V_x is V_0/e and can be calculated with:

$$\vartheta = \sqrt{\frac{\varepsilon_0 R}{2F^2} \frac{\kappa' T}{c_0 z^2}} = \sqrt{\frac{\varepsilon_0 k}{2e_0^2 N_{av}} \frac{\kappa' T}{c_0 z^2}} \tag{15}$$

where $N_{av} = 6.022 \cdot 10^{23}$ 1/mol is Avogadro's number. The exponential decrease of the potential described in Equ. 1 to 8 is true for the diffuse layer in Fig. 11(first of the three graphs). In the Stern layer, the potential decrease is linear, because in the vicinity of the solid particle, the counter-ions are interfering which prevents closer packing.

3.3.1 Influence of pH and Ionic Concentration

As evident in Fig. 11, the structural charge of the particle is compensated by counterions (which can be hydrated). The hydrated ions regularly move in and out of the double layer driven by

thermal agitation and abundance of counterions. Small cations (assuming negative particle charge) with high valence are positioned closer to the particle surface, because their size allows close packing and the high charge gives higher Coulomb attraction. Aluminum is an example for an ion that allows very close packaging due to its size but more importantly the charge of +3. The following sequence orders cations by their tendency to position themselves in the vicinity of the particle surface:

$$Al^{3+} \rightarrow Cu^{2+} \rightarrow Ca^{2+} \rightarrow Mg^{2+} \rightarrow K^+ \rightarrow Li^+ \rightarrow Na^+$$
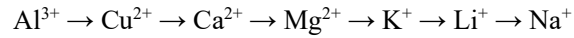
This concept is important to the measurement of particle charge (see Fig. 12 later in this chapter), because generally the structural charge cannot be measured directly. Instead, counterions/hydrated counterions close to the surface influence the measurement of surface charge. Ions on the right side of the sequence above can even lead to a charge reversal of the measurement compared to the actual structural charge of the particle.

Additionally, the structural or permanent mineral charge σ_0 is influenced by the abundance of H^+ and OH^- or simply by the pH of the electrolyte. In clay particles with negative surface charge, the terms protonation and deprotonation apply. The first term describes the abundance of H^+ in the electrolyte, which adsorb at the termination site with negative charge:

$$M - OH^- - H^+ \rightarrow M - HOH$$
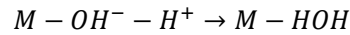
where M is a metal. Deprotonation occurs, if OH^- molecules are in the majority, compared to H^+ ions. In this case the OH^- molecules tend to remove H^+ from water molecules, decreasing the charge of particle close to its surface.

Together, cation complexation (Δq) and protonation and deprotonation (σ_H) compensate the structural charge of the mineral to fulfill the criterium for electroneutrality:

$$\sigma_0 + (\sigma_H + \Delta q) = 0 \tag{16}$$

It is impossible to measure the charge of the particle at zero distance from the surface. Instead, the charge is commonly defined at two distances away from the surface called the "point of zero charge" and the "isoelectric point" (Sposito 1998). The first one is defined as the pH at which the Stern potential is zero. The isoelectric point on the other hand is the pH at which the potential at the shear plane is zero (see Fig. 12). It is commonly referred to as the zeta potential and the phenomenon that allows to measure it is electrophoresis: an external electrical field applied on a clay particle suspended in electrolyte leads to a gradual movement of the particle towards one of the electrodes accompanied by a regular exchange of ions in and out of the double layer. Fig. 12 illustrates this phenomenon:
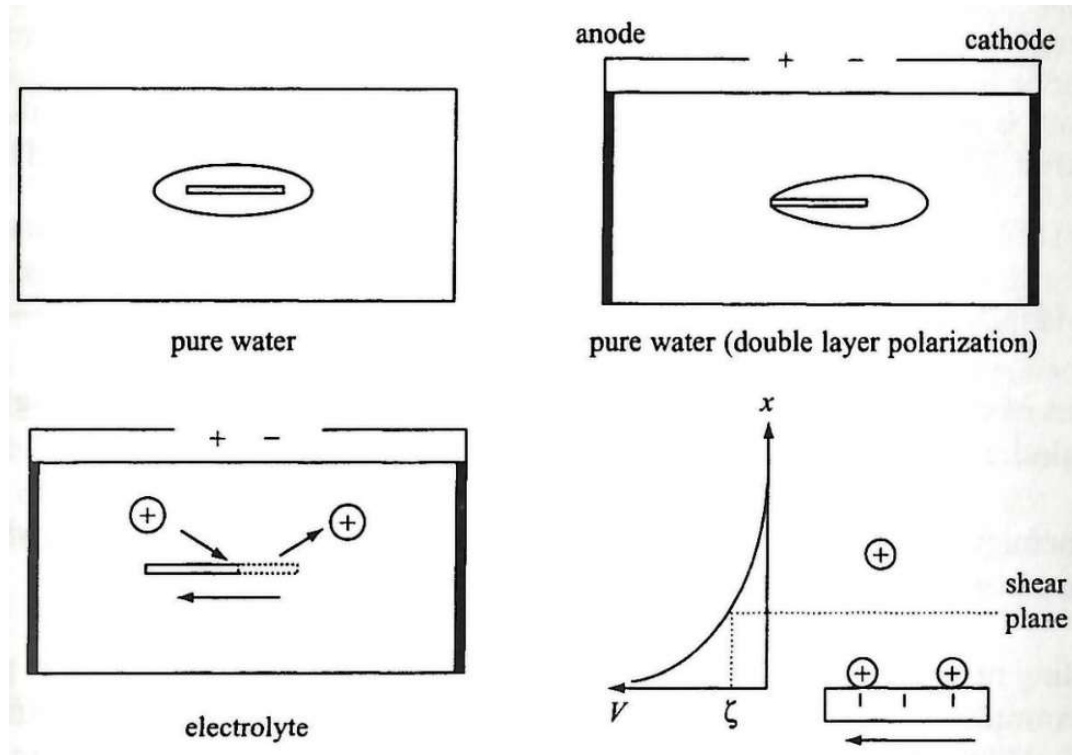
Figure 12: Electrophoresis of a clay particle and its double layer (Santamarina, Klein et al. 2001)

The zeta potential ζ can be calculated from

$$\zeta = 4\pi\eta\frac{U}{\varepsilon'} \tag{17}$$

where is the dynamic viscosity, ε' is the permittivity of the dispersed medium and U is the velocity of movement.

The measurement of the zeta potential of particles within an electrolyte allows one to interpret the influence of cation complexation and protonation and deprotonation on the charge of the particle at the shear plane. Fig. 13 shows qualitatively the change of zeta potential as a function of pH (a) and concentration of salts dissolved (b). Generally, ζ decreases with increasing pH of the electrolyte, which can be explained by the decrease in H^+ leading to deprotonation of the mineral surface. Cation adsorption is likely at O^{2-} termination sites, common for 2:1 minerals like Illite or Montmorillonite. The same minerals lack OH^- termination sites on the face sites (silica tetrahedral), which makes them less sensitive to pH compared to 1:1 minerals.
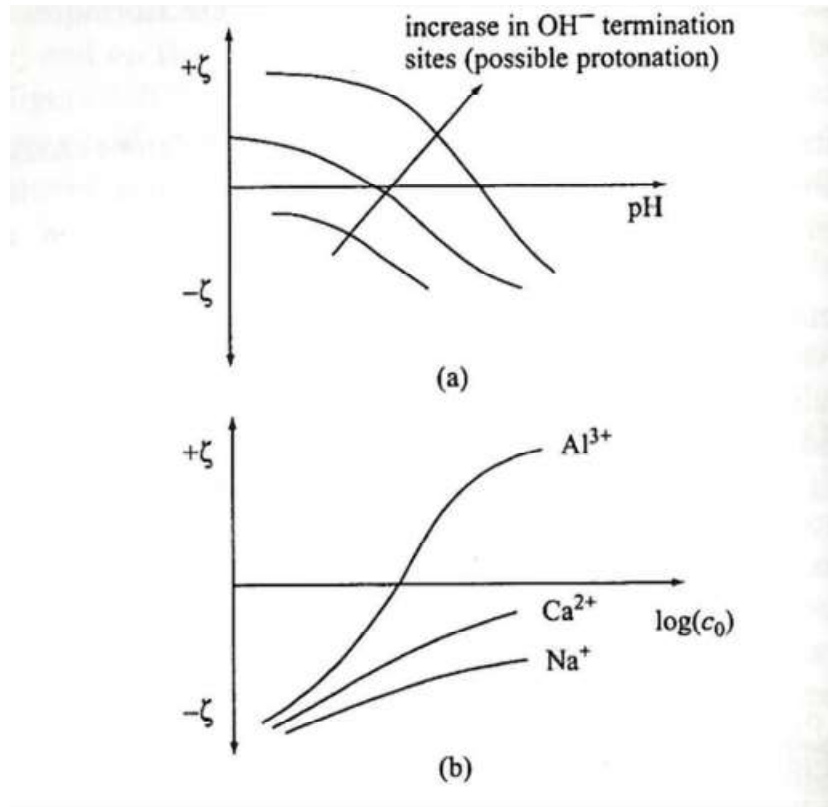
Figure 13: Qualitative zeta potential of clay minerals as a function of pH (a) and ionic strength (b)
(Santamarina, Klein et al. 2001)

Edge and face isoelectric points can differ from each other, due to the difference in the mineral structure at the edges. Kaolinite for example shows an edge IEP of 7.2, while the face IEP is around 4. Face to edge attractions through Colombian forces can be the result due to opposite charges.

3.4   Interparticle Forces

So far, the interaction between particle and surrounding fluid has been investigated. However, the experiments described in this thesis, were usually conducted with an excessive quantity of mineral particles, so that the amount of the solids is not the limiting factor in the experiments.

Coulombic forces, as mentioned in the previous chapter, are relevant to clay minerals through attraction between edge and face parts of the mineral assuming opposing charges:

$$F = \frac{1}{4\pi\varepsilon_0\kappa'}\frac{q_1q_2}{r^2} \tag{18}$$

However, two other contradicting forces make up the bulk of the forces that apply to clay minerals: Van der Waals-attraction and double layer repulsion. The two forces have long been assumed to be crucial to determine the behavior of colloidal particles, until Hamaker (1937)

computed the potential energy of particles as a function of their distance. As an example, Equ. 19 represents the attractive force between two circular parallel discs due to Van der Waals Forces (Israelachvili 2011):

$$F_{vdW} = \frac{1}{24} \frac{A_h}{x^3} d^2 \qquad (19)$$

where A_h is the Hamaker constant, which modifies the Van der Waals attraction in vacuum depending on the dielectric permittivity of the electrolyte. Changes in ionic concentration have little effect on the Van der Waals attraction.

Double layer repulsion is caused by the displacement of hydrated ions and water molecules within the double layer around charged particles (Chapt. 3.3). The displacement reduces the shielding function of the double layer and causes electrostatic repulsion between equally charged particles. For circular parallel discs the following relationship applies (Israelachvili 2011):

$$F_{DL} = 16\pi RT c_0 d^2 e^{-x/\vartheta} \qquad (20)$$

The strength of the repulsion is strongly influenced by ionic concentration of the electrolyte, as it directly influences the Debye-Hückel length or the size of the double layer around the particle (evident in Equ. 15). Higher concentrations decrease its size and therefore lower the repulsion. This gets evident, when we combine the two contradicting forces as suggested in the DLVO theory, named after Deraguin and Landau (1941) and Verwey (1947) and Overbeek.
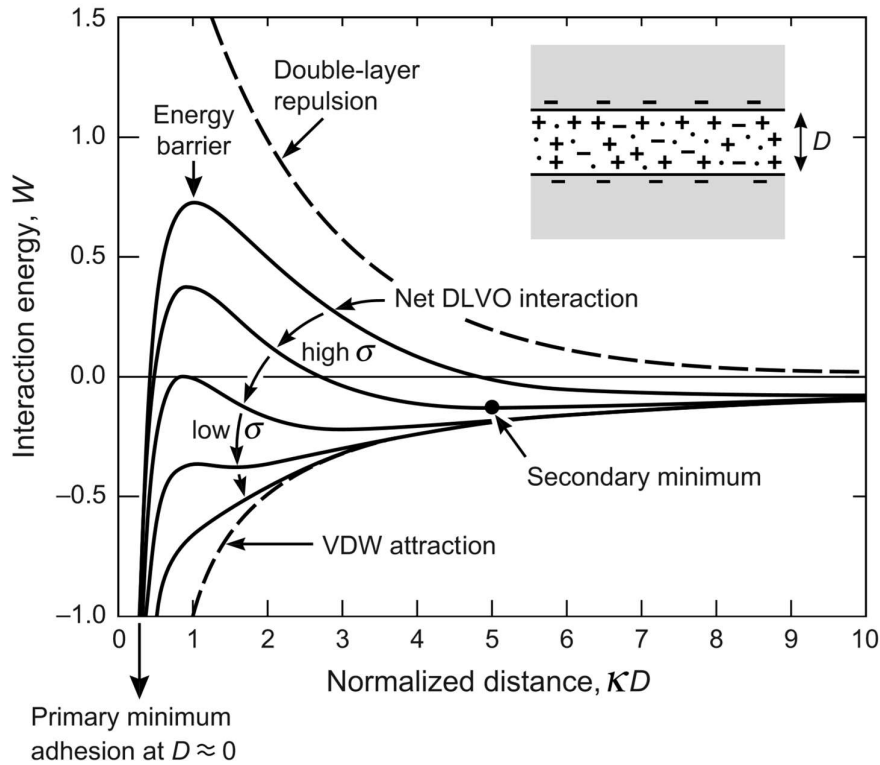
Figure 14: DLVO-theory combining Van der Waals-attraction and double layer repulsion
(Israelachvili 2011)

Fig. 14 schematically shows the interaction energy between two particles in a 1:1 electrolyte. It illustrates, that the Van der Waals-attraction always exceeds the double layer repulsion at very small distances, which can be explained by the exponent of the distance beneath the fraction line in Equ. 19.

The primary energy minimum is at close to zero distance, where the particles are in contact with each other and the Van der Waals interaction is near its maximum. Particles with a low surface charge density in a high ionic strength environment (meaning small double layers) have low energy barriers allowing them to reach the primary energy minimum and therefore aggregate.

For certain ionic concentrations secondary minima exist (mentioned in Chapt 2.2), that allow the particles to remain at a certain distance to each other in a metastable thermodynamic equilibrium. The higher energy barrier prevents the particles from reaching the primary minimum. Instead it is more likely for the particles to disperse in solution and reach a kinetic equilibrium (Israelachvili 2011).

3.4.1 Particle Associations and Fabric Maps

The preceding chapters have shown the general influence of pH and ionic concentration on the interaction between normal particles. It has been shown experimentally, that different kinds of associations of particles exist:

	Edge-to-face flocculation (EF): Colombian attraction between opposing charges of edges and faces of separate particles. EF only occurs at pH values between the edge isoelectric point and the face isoelectric point and is common for relatively thick particles like Kaolinite, where the edge charge of the mineral has significant influence on the behavior of the clay mineral. EF suspensions show higher values of shear resistance compared to solutions with dispersed particles.
	Face-to-face aggregations (FF): surfaces of the same charge are subject to Van der Waals attraction and double layer repulsion, described in the previous chapter as the two forces of the DLVO-theory. High ionic concentrations decrease the size of the double layer, thus promote FF aggregation. At pH values between the edge and face IEP, at which edges are positively and faces negatively charged, shifted FF aggregation is observed.
	Edge-to-edge flocculation (EE): intermediate condition between EF flocculation and FF aggregation caused by Van der Waals attraction. It occurs at pH values close to the IEP.

All the configurations above can be found in Kaolinite (see Fig. 15). The threshold between EF flocculation and FF aggregation at which EE flocculation occurs is between 0.1 and 0.15 mol/L. One distinct feature of Kaolinite is the gap between face and edge IEP that allows EF flocculation.
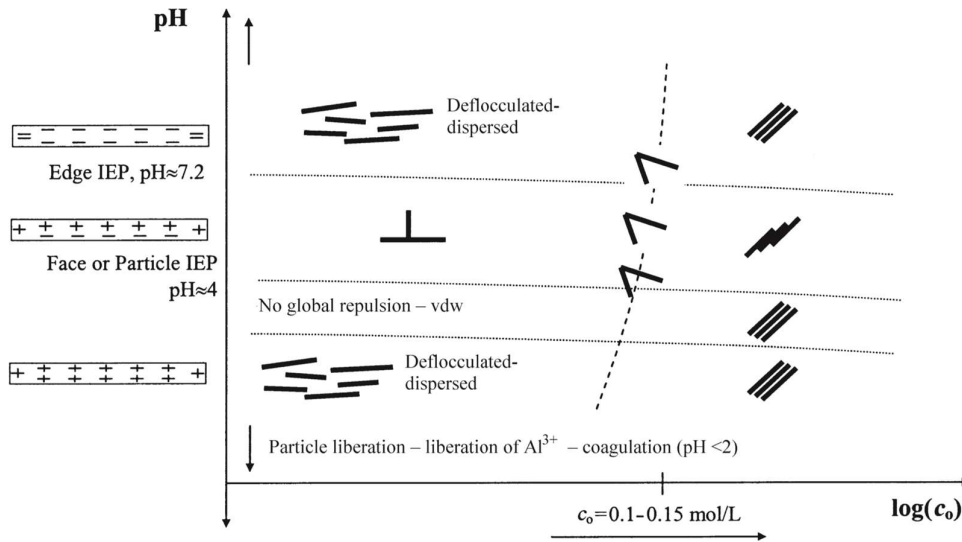
Figure 15: Postulated particle associations of Kaolinite as a function of ionic concentration and pH (Santamarina, Klein et al. 2002)

Kaolinite associations and their dependence on ionic strength and pH has been tested experimentally (Palomino, Santamarina et al. 2005). Sedimentation, viscosity and liquid limit tests are used to identify the presented regimes. As an example, the settling speed in the first test gives insight in the degree of agglomeration. Denser structures settle faster according to Stokes law (see Chapt. 4.2). The results agree with the tendencies presented in Fig. 15 above and emphasize the high influence of pH at lower ionic concentrations.

Montmorillonite shows similar tendencies but the thresholds at which particle associations change differ (see Fig. 16). Here, EE flocculation occurs between 0.005 and 0.3 mol/L. EF flocculation is restricted by the insignificant edge charge that is covered by the face charge of the particle.
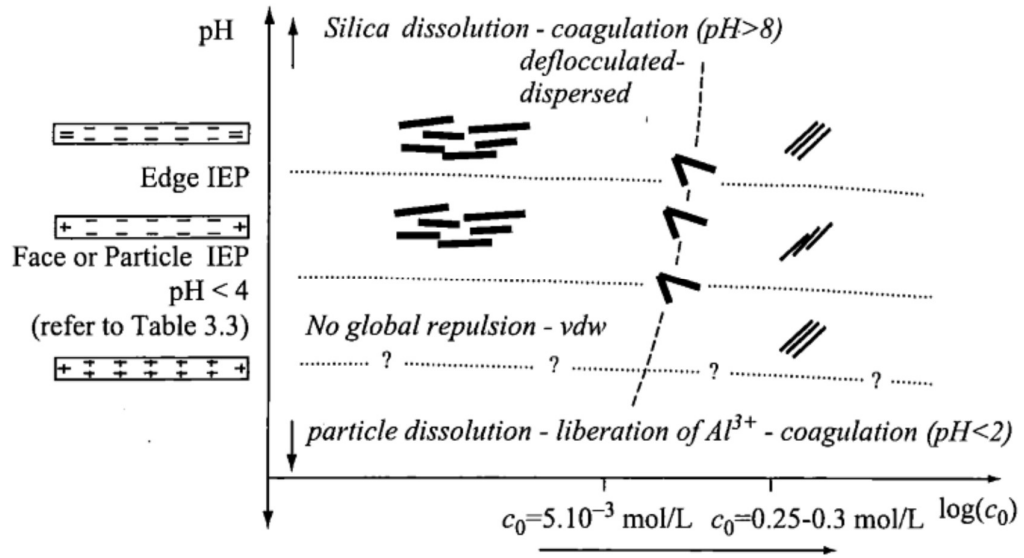
Figure 16: Postulated particle associations of Montmorillonite as a function of ionic concentration and pH (Santamarina, Klein et al. 2002)

The type of particle association defines certain properties of the suspension, like the density of the sediment or its viscosity. FF networks tend to have a higher density of particles than EF or EE suspensions, which have higher void ratios.

<div align="right">

Chapter 4

</div>

Sedimentation Tests

Sedimentation tests are widely used to investigate particle size and other soil properties. Here they are used not only to observe the behavior of the particle within a fluid, but also to investigate the behavior of particles at different fluid interfaces similar to the flotation test by Fürstenau (Chapt. 2.3.1).

4.1 Particles at Fluid Interfaces

To understand the behavior of particles at fluid interfaces a single particle at the oil and water interface is investigated. Fig. 17 shows a single solid, spherical, homogeneous particle at an oil-water interface, with a density higher than both fluids:

$$\rho_p > \rho_w > \rho_o$$

The fluid interface is assumed to be flat before the attachment of the particle and disturbed by gravitational force pushing the particle downwards and by the interfacial tension establishing a contact angle θ on the surface of the solid after the attachment. The vertical distance of the circle of contact, where all three phases meet, compared to the undisturbed interface is z_c.
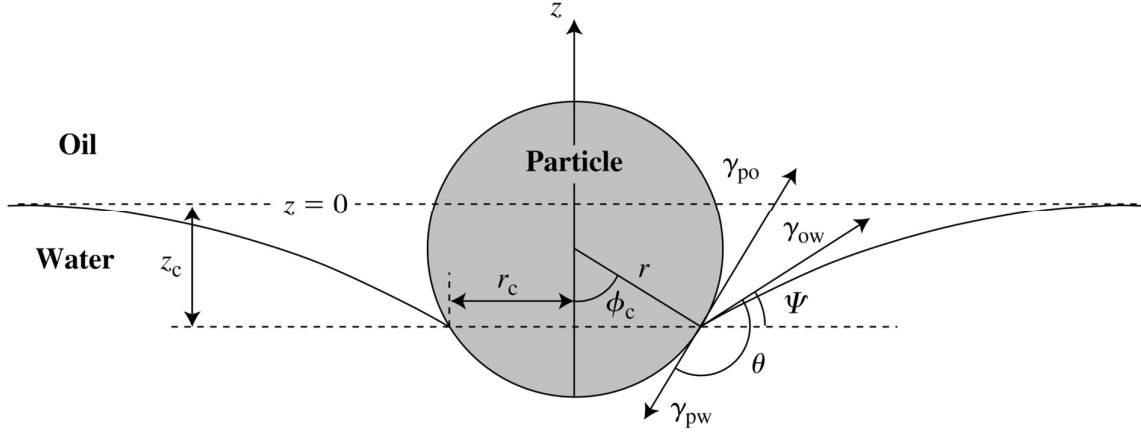
Figure 17: Spherical particle at an oil-water interface (Binks and Horozov 2006)

r_c is the radius of the same circle and defined as the product of the particle radius r and the sinus of the angle Φ_c, which describes the three-phase contact point, measured from the lowest point of the sphere.

$$r_c = r \cdot \sin \Phi_c \tag{21}$$

γ_{po}, γ_{pw} and γ_{ow} are the interfacial tensions introduced with Young's equation of contact angle introduced in Chapter 2 and the angle Ψ, a geometrical construct from θ and Φ_c is a measure of deviation from horizontality of the oil-water interface at the three-phase intersection.

$$\Psi = \Phi_c + \theta - 180° \tag{22}$$

At equilibrium the sum of the forces acting on the particle must be zero. The torsional relationships and the horizontal forces are not further investigated, because any possible results are already obvious due to the symmetry of the particle and the surrounding interface. The vertical net forces are more useful and can be segmented into three parts.

$$F_\gamma + F_p = m \cdot g \tag{23}$$

F_γ is the vertical component of the capillary force. Capillary force (see Chapter 2) is the result of an interfacial tension acting on a unit length, in this case a circle with a contact line length of $2\pi r \sin \Phi_c$.

$$F_\gamma = \gamma_{ow} \cdot 2\pi r \sin \Phi_c \sin \Psi = -\gamma_{ow} \cdot 2\pi r \sin \Phi_c \sin(\Phi_c + \theta) \tag{24}$$

F_p accounts for the buoyancy of the sphere and the additional hydrostatic pressure from the depression of the liquid interface by z_c.

$$F_p = \rho_w V_{pw} g + \rho_o V_{po} g - (\rho_w - \rho_o) g z_c A_c \tag{25}$$

where A_c is the area enclosed by the circle of three-phase contact:

$$A_c = (r \cdot \sin \Phi_c)^2 \pi \tag{26}$$

and V_{pw} and V_{po} are the volumes of the sphere submerged in water and oil respectively:

$$V_{pw} = \frac{r^3 \pi}{3}(2 - 3\cos \Phi_c + \cos^3 \Phi_c) \tag{27}$$

$$V_{po} = \frac{4r^3 \pi}{3} - V_{pw} \tag{28}$$

The right part of Equ. 23 is simply the gravitational force of the particle pointing downwards. The mass of the sphere is:

$$m = \rho_p \frac{4r^3 \pi}{3} \tag{29}$$

Substituting Equations (24) to (29) into (23) gives:

$$-\gamma_{ow} \cdot 2\pi r \sin \Phi_c \sin(\Phi_c + \theta) + \rho_w \frac{r^3 \pi}{3}(2 - 3\cos \Phi_c + \cos^3 \Phi_c)g$$
$$+ \rho_o \left(\frac{4r^3 \pi}{3} - \frac{r^3 \pi}{3}(2 - 3\cos \Phi_c + \cos^3 \Phi_c) \right)g$$
$$- (\rho_w - \rho_o)gz_c(r \cdot \sin \Phi_c)^2 \pi = \rho_p \frac{4r^3 \pi}{3}g$$

$$\tag{30}$$

Rearranging and simplifying Equ. (30) is shown in detail in Appendix (7.5):

$$\sin \Phi_c \sin(\Phi_c + \theta) = -\frac{B}{6}\left[4\frac{\rho_p - \rho_o}{\rho_w - \rho_o} - (1 - \cos^2 \Phi_c)(2 - \cos \Phi_c) + 3\frac{z_c}{r}(\sin \Phi_c)^2 \right] \tag{31}$$

Where B is the Bond number, sometimes called the Eötvös number:

$$B = \frac{(\rho_w - \rho_o)r^2 g}{\gamma_{ow}} \tag{32}$$

The Bond number is a dimensionless property describing the impact of the gravitational force against the force due to interfacial tension.

For the particle in order to stay at the interface of oil and water, the capillary force F_γ needs to point upwards, opposing the direction of the gravitational force. Subsequently, following Eq. (4) $\Phi_c + \theta \geq 180°$ and $\Phi_c \leq 180°$ must be true, restricting the left-hand side of Eq. (11) to a value between -1 and 0. Solutions for Eq. (11) therefore only exist if B is not larger than a certain threshold or to put it in simpler words, the particle will not attach to the interface and but sink instead, if it is too heavy. The threshold for the particle for a given contact angle, interfacial tension and density of the liquids to stay attached at the interface is obviously very important, especially in applications like flotation. However, an analytical solution does not

exist for spherical particles. Other authors (Kralchevsky and Nagayama 2001) have proposed approximate analytical and numerical solutions.

The problem can be simplified, if the deformation of the fluid interface caused by the gravitational force on the particle is neglected. This is acceptable for small particles. For air-water surfaces particles with a diameter smaller than 5 microns cause negligible deformation of the fluid interface (Kralchevsky and Nagayama 2001). The model illustrated in the Fig. 18 below is therefore acceptable.
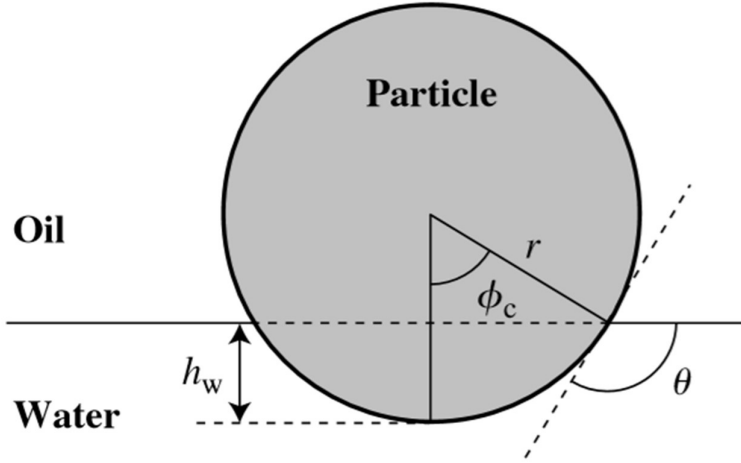
Figure 18: Simplified model for a small colloidal particle at a fluid interface (Binks and Horozov 2006)

Following the context in the Fig. 18 above, one can clearly see that there is direct relationship between the vertical position of the particle and its contact angle. Changing the wettability would therefore also change the vertical position.

$$h_w = r(1 + \cos\theta) \qquad (33)$$

However, this is not true if we look at the issue the other way around. The contact angle does not change if a manual force is applied on the particle, thus the simplification to disregard the influence of the particle on the liquid interface would not be applicable anymore ($z_c \neq 0$).

To circumvent this issue, an energy model comparing the free energy change from an equilibrium position of the particle at the fluid interface to a detached position, does not require intermediate positions to be considered. At equilibrium state, the free energy system $G^{(1)}$ is at its minimum, given by the following equation:

$$G^{(1)} = \gamma_{ow} A_{ow}{}^{(1)} + \gamma_{pw} A_{pw}{}^{(1)} + \gamma_{po} A_{po}{}^{(1)} \qquad (34)$$

The areas A_{ow}, A_{pw} and A_{po} describe the contact areas between oil-water, particle-water and particle oil respectively. After detachment of the particle from the interface to the oil phase that

lies above, there is no contact of the particle with the water phase anymore, simplifying the equation by a term:

$$G_o^{(2)} = \gamma_{ow} A_{ow}^{(2)} + \gamma_{po} A_p^{(2)} \tag{35}$$

Subtracting Eq. (145) from Eq. (15) gives the free energy of particle detachment into oil:

$$\Delta G_{do} = \gamma_{ow}\left(A_{ow}^{(2)} - A_{ow}^{(1)}\right) - \gamma_{pw} A_{pw}^{(1)} + \gamma_{po}\left(A_p^{(2)} - A_{po}^{(1)}\right) \tag{36}$$

where we can include a relationship of areas that must be true as well as using Young's Equation.

$$A_p^{(2)} = A_{pw}^{(1)} + A_{po}^{(1)} \tag{37}$$

$$\Delta G_{do} = \gamma_{ow}\left(A_{ow}^{(2)} - A_{ow}^{(1)}\right) - \gamma_{pw} A_{pw}^{(1)} + \gamma_{po}\left(A_{pw}^{(1)}\right) \tag{38}$$

$$cos\theta = \frac{\gamma_{po} - \gamma_{pw}}{\gamma_{ow}} \tag{4}$$

$$\Delta G_{do} = \gamma_{ow}\left(A_{ow}^{(2)} - A_{ow}^{(1)} + A_{pw}^{(1)} \cos\theta\right) \tag{39}$$

Conversely, the free energy of particle detachment into water is:

$$\Delta G_{dw} = \gamma_{ow}\left(A_{ow}^{(2)} - A_{ow}^{(1)} - A_{po}^{(1)} \cos\theta\right) \tag{40}$$

Or if Eq. (19) and (20) are combined:

$$\Delta G_{do} = \Delta G_{dw} + \gamma_{ow} cos\theta \tag{41}$$

For spherical particle, which has a total surface areas of $4\pi r^2$, leading to $A_{ow}^{(2)} - A_{ow}^{(1)} = \pi(r\,sin\theta)^2$ and $A_{pw}^{(1)} = 2\pi r^2(1 + cos\theta)$, the detachment energies are:

$$\Delta G_{dw} = \pi r^2 \gamma_{ow}(1 - \cos\theta)^2 \tag{42}$$

$$\Delta G_{do} = \pi r^2 \gamma_{ow}(1 + \cos\theta)^2 \tag{43}$$

Eq. (22) indicates that a particle that is hydrophilic and has a positive $cos\theta$, less energy is required to detach into water than into the oil phase. Equally, Eq. (43) shows that detachment into oil is easier for hydrophobic particles. To visualize this concept, Fig. 19 shows the minimum free energy of detachment into water and oil as a function of the contact angle.
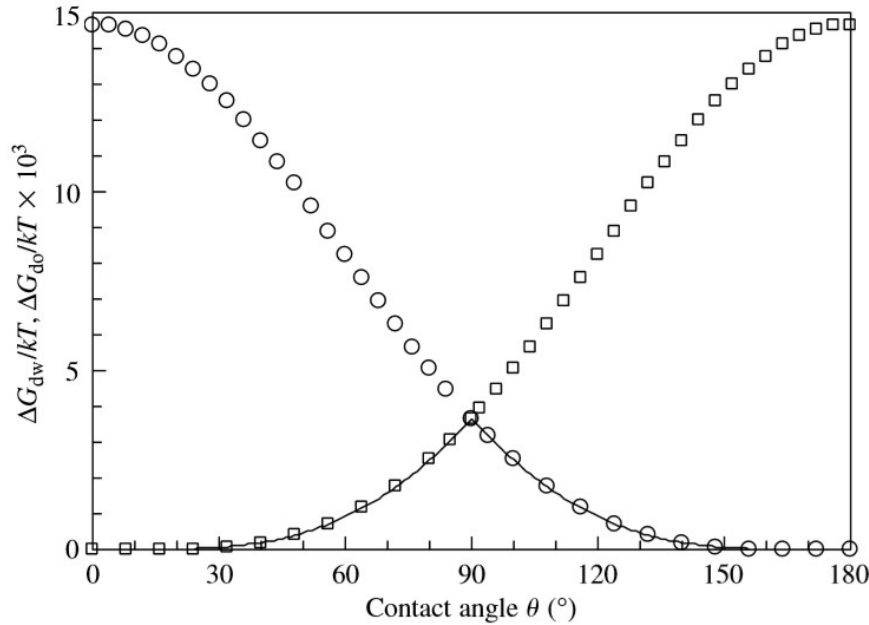
Figure 19: Free energy of detachment for a spherical particle into water (squares) and oil (circles) for a spherical particle with r=10nm and $\gamma_{ow} = 50mNm^{-1}$ (Binks and Horozov 2006)

To summarize, it is difficult for a spherical particle to leave an oil-water interface if the contact angle is close to 90°. Note that that deformation of the liquid interface can also be caused by non-uniform wetting of the particle surface or asymmetric fields around a charged particle. These causes have not been considered in the interpretation of experiments done in this thesis work. (Binks and Horozov 2006).

The immersion time of solids in water-ethanol mixtures was investigated by others to investigate the degree of hydrophobicity of homogeneous particles (Garbsva, Contreras et al. 1978) or to determine the distribution of the wettability of heterogeneous particles or an assembly of different kinds of particles (Fuerstenau, Diao et al. 1991). The latter case is commonly used to sort minerals of different particle sizes and wettabilities physically by film flotation.

4.2   Terminal Velocity of a Particle During Sedimentation

The approximate size of a particle can be calculated by measuring its terminal settling velocity in a liquid medium. It is a simple test, that is based on a force equilibrium of gravitational force acting downward, and buoyant and drag force acting upward.

$$mg - m'g = F_D \qquad (44)$$

$$\frac{\pi}{6}d^3\left(\rho_s - \rho_f\right)g = F_D \qquad (45)$$

where m is the mass of the particle, m' is the mass of the same volume of fluid, ρ_s and ρ_f are the densities of solid and fluid respectively, g is the acceleration from gravity and d is the particle diameter. The drag force F_D can be calculated from:

$$F_D = 3\pi\eta du \tag{46}$$

where η is the fluid viscosity and u is the terminal settling velocity of the particle. Merging Equ. (45) and (46) and transforming the equation so that the velocity is on one side, give:

$$u = \frac{(\rho_s - \rho_f)gd^2}{18\eta} \tag{47}$$

Note that this is only true for laminar flow (Reynolds number <0.25), low velocities so that inertia can be mitigated and spherical, smooth and rigid particles. Clay particles however are non-spherical, which makes an adaption necessary:

$$d_{st}^2 = \frac{d_v^3}{d_d} \tag{48}$$

where d_v is the diameter of a sphere with the same volume as the particle, d_d is the diameter of the sphere experiencing the same drag force as the particle moving at the same terminal velocity in the same fluid (Allen 2013).

As mentioned in Chapter 3.5, particles suspended in fluid associate in different structures depending on the ionic and pH environment of the liquid. Flocculated particles cannot be treated similar to solitary ones, when the particle diameter is calculated from Stokes' law. Their density changes with the degree of flocculation offering the possibility to identify different association regimes via sedimentation tests. In experimental studies it has been observed, that dispersed flocks settle slow, EF flocculated particles settle fast and FF aggregated particles settle very fast(Palomino 2003). Other relationships can be obtained from the following table:

Table 1: Sedimentation characteristics for different particle associations of Kaolinite (Palomino, Santamarina et al. 2005)

Sedimentation characteristics	Mode			
	Dispersed sedimentation	EF flocculation sedimentation	FF aggregation sedimentation	Mixed-mode sedimentation
Particle interaction	Minimal; any aggregates formed remain dispersed	Strong; flocs form readily	Strong; aggregates form readily	Minimal → floc/agg. formation
Suspension appearance	Milky with increasing density from top to bottom	Uniform density	Uniform density	Top to bottom increasing density → uniform
Supernatant liquid appearance	Cloud of suspended fine particles	Clear	Clear	Cloudy → Clear
Suspension-supernatant liquid interface	None	Well defined, moves downwards as flocs settle	Well defined, moves downwards as aggregates settle	None → well defined
Suspension-sediment interface	Well defined, moves upwards as sediment builds	None	None	Well defined → none
Settlement rate	Very slow	Rapid, constant	Very rapid, constant	Slow → rapid
Sediment formation	Particles settle into lowest possible position and according to size, largest first	Flocs settle in random pile	Aggregates settle according to size	Particles settle according to size → Formed flocs/aggregates settle uniformly
Sediment volume	Compact; strongly resists redispersion	Voluminous; easily redispersed	Compact to voluminous	Layer of compact sediment below layer of voluminous sediment

4.3   Experiment

Several different variations of water-based liquids, organic liquids and their interaction with various powders are captured in this series of sedimentation tests. The first test conducted, done with Kaolinite shall be called the base test and serve as guidance example with in-depth explanation of the steps involved. The solids, liquids and other test material used in the test series is described in more detail in the Appendix (7.6).

4.3.1 Setup

Three vials are mounted in front of the digital camera. A backlit panel placed behind the vials provides illumination during the capturing of the images. One vial is filled with 10ml water, one is filled with 10ml of kerosene, while the third vial is filled with 5ml of each liquid.

Figure 20: Sedimentation test on Kaolinite, (left): initial setup before adding kaolinite powder. 10ml of water in the left vial, 5ml of water below 5ml of kerosene in the second vial and 10ml of kerosene in the right vial. (right): Snapshot of the ongoing experiment 39 seconds after adding 0.5g of kaolinite powder to each vial

In the vial with both liquids present, it is worth noting that the water has been filled into the vial first, because its density is higher than that of kerosene. By filling in the heavier fluid first, the occurrence of bubbles of one liquid within the other one is prevented. As indicated by the meniscus in the left Fig. 20 above, the polypropylene vial promotes oil wetting behavior, which could lead to kerosene droplets sticking to the vial surface below the water-kerosene interface.

Next, 0.5g-portions of Kaolinite are slowly poured into the vial via funnel shaped plastic weigh boats. The height from which the powder is released is kept at a minimum, so that the kinetic energy does not influence the behavior of the solids at the air-liquid phase too much. The digital camera captures the experiments using backlight lighting to provide high contrast between the transparent liquids and the fairly light clay mineral colors. Interpretation of the experiments is aided by cutting several segments from the raw video shifting them in time so the point in time where the first powder particle touches the surface of the uppermost liquid is also the start of the video.

4.3.2 Results and Discussion

The base test described for kaolinite in 3.3.1 is also done for silica flour, illite, bentonite and Eagle Ford with three vials per test run with water, water-kerosene and kerosene as liquids respectively. The tests allow the observation of different powder particles not only within the liquids mentioned but also their behavior at three different fluid interfaces:

- Air-water interface
- Kerosene-water interface

- Air-kerosene interface

Silica Flour (after 40 sec.)	Kaolinite (after 39 sec.)	Illite (after 90 sec.)
Bentonite (after 77 sec.)	Eagle Ford (after 44 sec)	
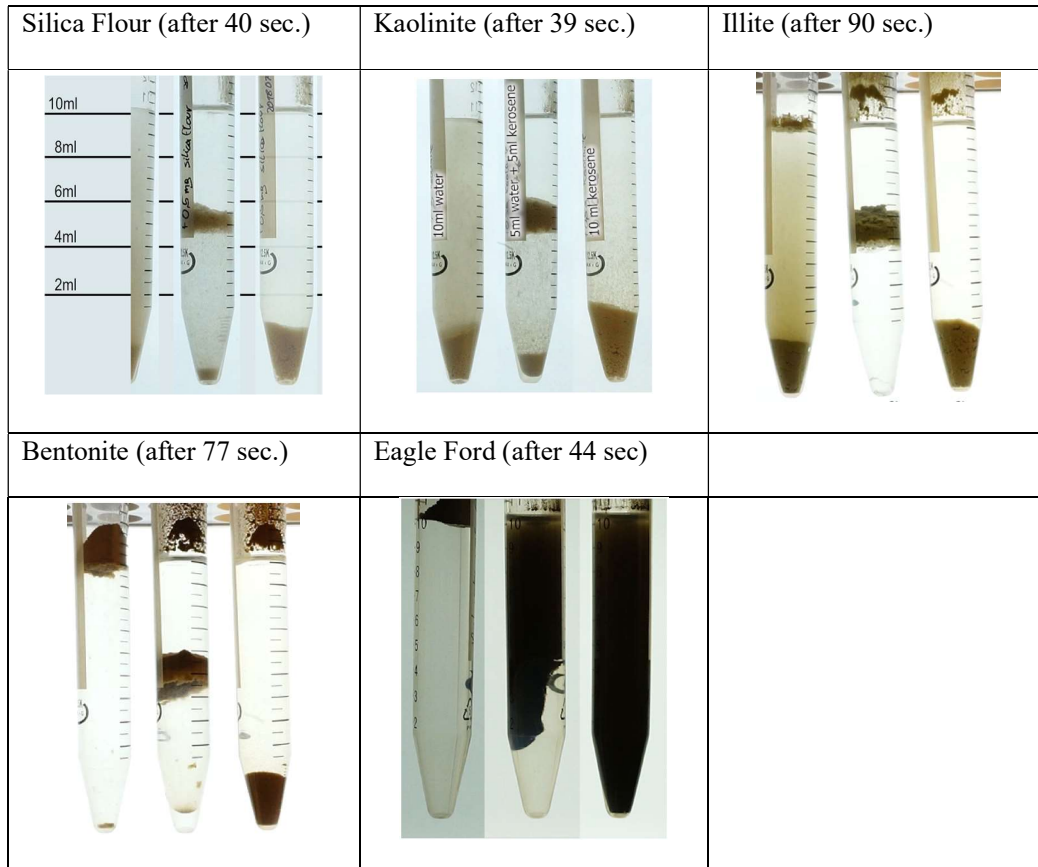
Figure 21: Overview of Sedimentation Test series on Silica Flour, Kaolinite, Illite, Bentonite and Eagle Ford in water (left image), kerosene (right image) and kerosene-water (center image)

Table 2: Settling times within pure liquids and residence times at the fluid interfaces for sedimentation test series

Powder	Air-Water Interface	Kerosene-Water Interface	Air-Kerosene Interface
Silica Flour	t→0	T=90min	t→0
Kaolinite	t→0	T=16min	t→0
Illite	t=90 sec	t→inf	t→0
Bentonite	t→inf	t→inf	t→0
Eagle Ford	t→inf	t→inf	t→0

Note that the viscosity of the liquids involved also influences both interface time and settling speed (Dymond, O/ye et al. 1994)

- $\mu_{water} = 1 mPa \cdot s @ 20°C$
- $\mu_{Kerosene} = 1.5 - 2 \ mPa \ (depending \ on \ the \ exact \ composition)$
- $\mu_{decane} = 0.92 mPa \cdot s @ 20°C$

4.3.2.1 Interface Residence Time

The hydrophilic particles Silica Flour and Kaolinite have air-water interface times close to zero. The energetic model discussed in Chapter 4.1 states that wettabilities involving contact angles smaller than 90° favor detachment of particles into water rather than oil. Same is true for an air-water system where air is the non-polar medium. That means, that one can expect that hydrophilic particles pass through fluid-water interface ($\rho_{fluid} < \rho_{water}$) more likely than hydrophobic particles. The Eagle Ford for example does not penetrate the water and instead stays on top of the air-water interface. It is most likely hydrophobic due to its origin (see Appendix 7.6.1).

Illite and Bentonite although generally hydrophilic also show non-zero interface times during the sedimentation test series. This contradicts the previous statement, so investigation of possible other effects is necessary. The video file indicates a certain increase in volume compared to the Eagle Ford powder (the only other powder staying at the air-water interface). This is, because of swelling of the clay minerals exposed to low-saline water. Especially bentonite expands extensively and in a way that blocks further movement of the particles downwards, allowing only very little powder material to reach the bottom of the vial. Illite shows some swelling as well, but not in a way that completely blocks vertical movement. The almost spherical assembly visible in the Fig. 22, slowly crumbles as more water invades. Swelling therefore delays the transition from air to water but does not block it in a way that is observed with hydrophobic Eagle Ford.

Illite (after 41 sec.)	Bentonite (after 73 sec.)	Eagle Ford (after 44 sec.)
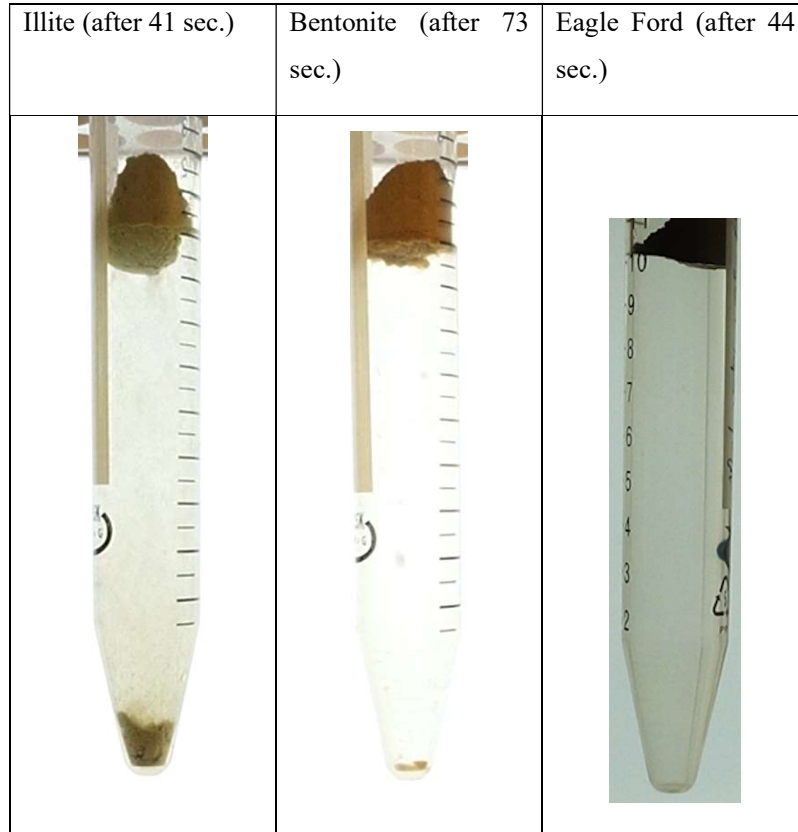
Figure 22: Sedimentation test of Illite, Bentonite and Eagle Ford in water after 41 sec.

The air-kerosene interface (see right vials in the overview of the sedimentation experiments shown in the Table above) is zero for all powder types. Again, this contradicts a previous observation that wettability is decisive to the behavior at the interface. In fact, the particle size, the density difference between the two fluids and the surface tension also need to be considered. As established in Chapter 4.1 the Bond number combines these two variables as one comprehensive variable.

$$B = \frac{\Delta \rho_{fluids} r^2 g}{\gamma} \tag{32}$$

Low surface tensions decrease the maximum particle size that can be supported by the fluid interface. The surface tension of kerosene is only a third of the surface tension of water explaining the low residence time at the air-kerosene interface compared to the air-water interface:

- $\gamma_{air-water} = 72.86 \; mNm^{-1} \; @ \; T = 20°C$ (Adamson and Gast 1967)
- $\gamma_{decane-wate} = 52.22 \; mNm^{-1} \; @ \; T = 20°C$ (Zeppieri, Rodríguez et al. 2001)
- $\gamma_{air-kerosene} = 23.83 \; mNm^{-1} \; @ \; T = 20°C$ (surface-tension.de)

So, compared to the air-water interface, the Bond number at the air kerosene interface is increased by the change in interfacial tension and decreased by the slight decrease in the fluid

density difference. Overall, the Bond number must be higher, hence fewer particles stay at the interface.

The density difference between kerosene and water with $0.8 g/cm^3$ and $1 g/cm^3$ respectively is quite low. Consequently, the Bond number is lower compared to the Bond numbers at the air-water and the air kerosene interface, which as discussed, hinders particles of passing through the interface easily, hence why the measurement results show only non-zero interface times at the kerosene-water interface.

4.3.2.2 Settling Speed

The test setup is not ideal in observing settling speed, which is commonly observed through sedimentation tests in which particles and liquid are mixed thoroughly. The physical principles of the relation of the size of a particle and its terminal velocity (see Chapter 4.2) requires laminar flow. By pouring a significant number of heavy particles into the vials at once, as done in the experiments here, turbulent flow is dominant. After some timer however, the turbulences diminish, and laminar flow dominates. A direct measurement of the speed of single particles has not been feasible due to technical limitations (explained in detail in Chapter 7.1), but qualitative observations from the video files and approximate settling times, allowing assessment of the settling behavior within the liquids.

Table 3: Overview of settling speed and structure observed during the sedimentation test

Solid	Kaolinite	Silica Flour	Kaolinite	Silica Flour
Liquid	Water		Kerosene	
Particle interaction	Limited - particles predominantly dispersed		High – agglomerates form	Very high – flocks form
Suspension appearance	Milky		clear	clear
Settlement rate	Slow		fast	Very fast
Sediment	compact		Voluminous	Voluminous

The settling of Kaolinite and Silica Flour in water is similar. In both cases no visible aggregations occur. Instead a cloudy suspension slowly settles to form a compact structure at the bottom of the vial. Both particles types settle much faster in kerosene. Kaolinite forms aggregates, which not only settle faster than the dispersed particles in water, but also make the suspension appear cleaner and not milky like at the experiment with water. Silica flour in

kerosene agglomerate even more, forming large flocks which fall to the bottom of the vial immediately. Larger particles generally sink faster (see Chapter 4.2)

The volume after sedimentation is larger for kerosene than for water, because the agglomerates maintain their structure allowing fairly large pores filled with fluid.

Kaolinite in water after 44 sec	Kaolinite in kerosene after 20 sec.	Silica Flour in water after 44 sec	Silica Flour in kerosene after 20 sec.

Figure 23: Snapshot of settling behavior of Kaolinite and Silica Flour during sedimentation test

In conclusion, different particles associations can be observed. They are summarized in Table 1 and explained in more detail in Chapter 3.5.

Chapter 5

Pickering Emulsion Tests

Although first mentioned by Ramsden (1903), emulsions stabilized by solid particles adsorbed at the interface of two fluids are named after Pickering (1907). In his paper published over a hundred years ago, he proved the stabilization of oil droplets within water through adsorption of several types of particles on the oil-water interface and identified advantages to surfactant-based emulsions.

Several particle types can stabilize emulsions. The main focus of this thesis is on colloidal particles of simple spherical shapes (see Chapter 4.1). Janus particles (see Fig. 24 (b), which consist of surface areas of different physical properties, are investigated in numerous research papers, but are beyond the scope of this thesis. The third particle, illustrated in Fig. 24 (c), shows a classical surfactant molecule, which similarly to the Janus particle consists of both hydrophilic and hydrophobic parts.

Hydrophobic

Hydrophilic

Figure 24: (a) homogeneous colloidal particle, (b) heterogeneous colloidal particle and (c) surfactant molecule (Binks and Horozov 2006)

5.1.1 Emulsion Type

For conventional chemical surfactants the solubility of the surfactant particles determines the emulsion type. Water soluble hydrophilic particles produce oil-in-water emulsions, while

hydrophobic particles lead to water-in-oil emulsions. This is determined by the energy of head and tail of a surfactant molecule and defined as Windsor ratio.
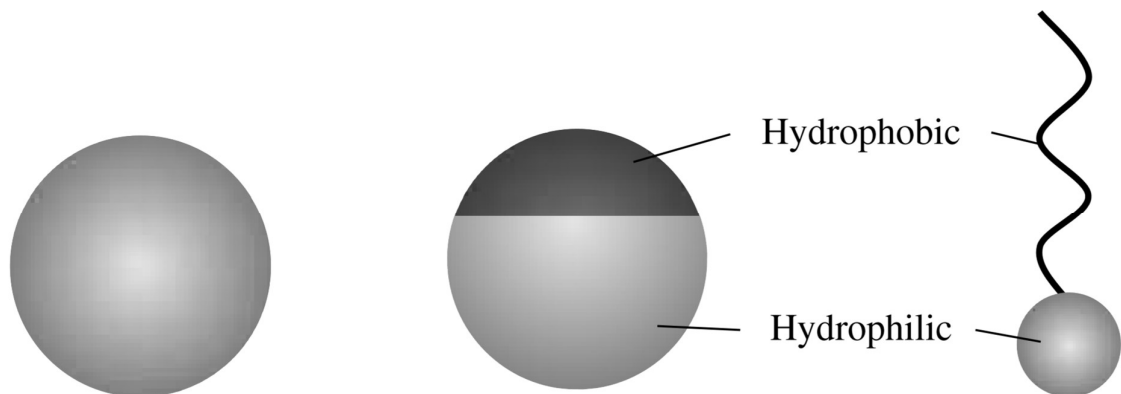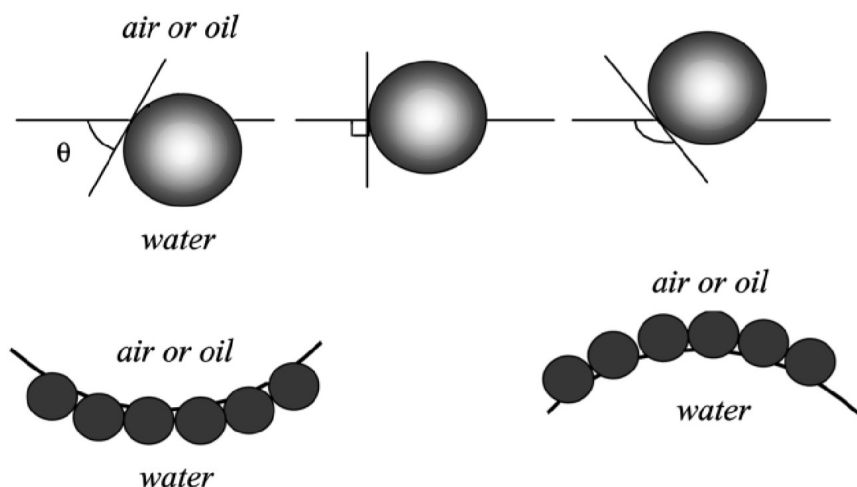

Figure 25: The emulsion type depends on the relative position of a particle at an interface and thus on the wettability of the particle (Aveyard, Binks et al. 2003).

Pickering emulsions (Fig. 25) work similar. Particles at the oil and water interface that show a contact angle in water that is smaller than 90° (which we defined as the definition for hydrophilic particles in Chapt. 1.3) tend to form emulsions of oil-in-water. Vice versa, particle that establish contact angles of more than 90° form emulsions of water-in-oil (Chevalier and Bolzinger 2013). The emulsion type therefore can give information on the wettability type of the particle. Other authors (Kralchevsky, Ivanov et al. 2005) suggest that the monolayer could the decisive factor behind the emulsion type, by minimizing its bending energy.

5.1.2 Phase Inversion and how to influence it

Surfactant based emulsion are more stable if hydrophobicity or hydrophilicity of the surfactant particle is high. This behavior opposes typical stability behavior of Pickering emulsions, which are usually more stable with contact angles closer to 90° (Chevalier and Bolzinger 2013).

Surfactant-based emulsions are influenced by the particle shape and the salinity of the water. This changes droplet size and rheological properties of the final emulsion, but hardly leads to radical phase inversions. On the contrary, Pickering emulsions can be easily influenced to an extend in which phase inversion can occur. This phenomenon is called phase inversion and can happen within small changes of θ_w. Modifying the wettability of the solid particles, adjusting the relative volumes of oil and water or alternating the phase which the solids are contacting first, are all factors ultimately influencing the properties of the emulsion (Chevalier and Bolzinger 2013).

5.1.3 Emulsion Droplet Size

For Silica Flour, which is closer to a spherical particle than the clay minerals, the general idea, that a higher number of silica particles leads to more surface coverage of the dispersed phase within an emulsion and thus decrease the average emulsion droplet size, has been observed experimentally (Frelichowska, Bolzinger et al. 2010). Over a large range of silica mass, the following equation describes the linear relationship:

$$emulsion\ diameter = \frac{6}{\rho_{oil} a_{solid}} \frac{M(oil)}{M(solid)}$$

where a_{solid} is the interfacial area per unit mass of silica at full coverage. This is not true for very high mass ratios of oil to silica where emulsification is incomplete or too low ratios, where excess silica coexists within the emulsion.

5.1.4 Rheology of Pickering Emulsions

Aggregation of dispersed droplets coated with solid particles can influence the viscosity of the emulsion. It occurs, if an excess volume of solids stays within the continuous phase at a certain salinity level that mitigates electrostatic repulsions by the charges of the solid particles (Binks, 2007)

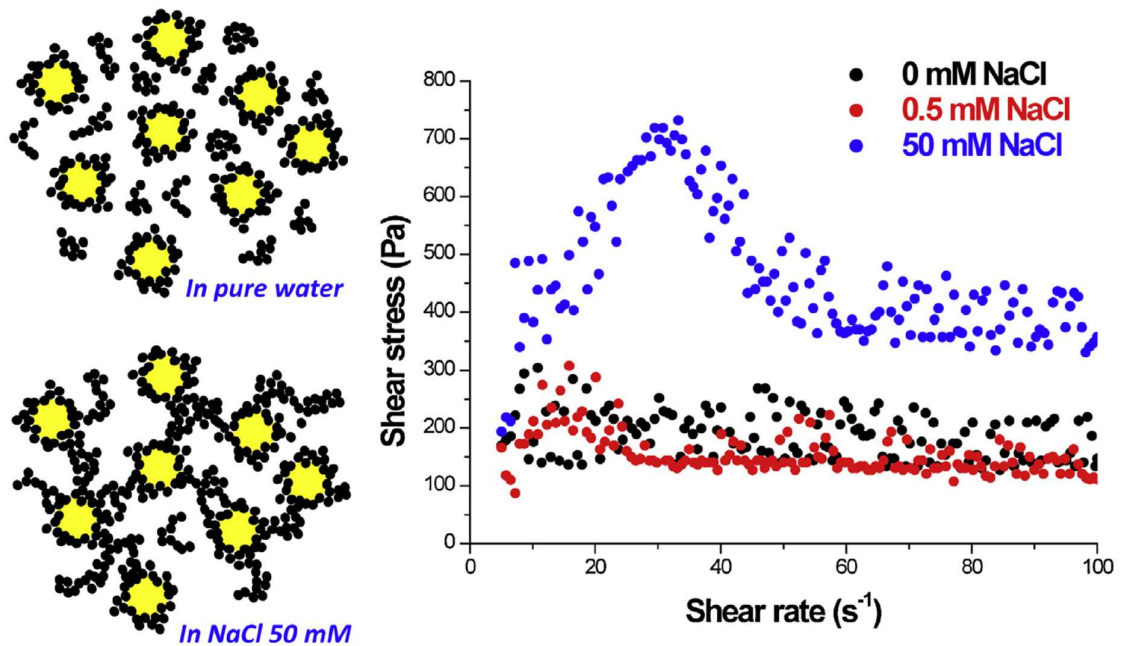*Figure 26: Rheological behavior of an oil-in-water Pickering emulsion of silicone oil (10% volume) and brine (varying concentrations of NaCl) stabilized by silica particles (5%) (Chevalier and Bolzinger 2013)*

Excess solid particles disperse in the aqueous phase at low levels of salinity. In emulsions with high ionic strengths free solids aggregate and form connected structures within the continuous

phase. Fig. 26 shows the presumed structures for oil-in-water Pickering emulsions with low and high levels of salinity and the change in the rheological behavior. High NaCl content leads to thickening of the emulsion preventing early creaming and therefore a more stable emulsion. Very high ionic strengths can form gels with a yield strength and elastic behavior (Chevalier and Bolzinger 2013).

5.2 Experiment

Pickering emulsion are not only an alternative to surfactant-based emulsions, they also offer insight into the wettability of the solids. The following test series investigates Pickering emulsions based on the emulsion type (oil-in-water or water-in-oil) and thus identifies the wettability of the solid. Emulsion features like volume, solid content and bubble size are also analyzed.

5.2.1 Setup

The setup of emulsions is a continuation of the sedimentation test series. After completing video capturing the sedimentation tests, the same vials are tilted upside down five to eight times. The vials are placed in a bracket and time lapse photography with a digital camera is started. After one hour, the vials are tilted again. A total of four one-hour long runs are done to establish an equilibrium and to allow clay minerals to swell. Then, the actual run starts und is given enough time – usually overnight – after which the vials are stored. After a few days or weeks, the vials are checked to confirm long term stability of emulsions.

5.2.2 Change of Settling Speed from Clay Swelling

This is demonstrated by the following image series, which shows kaolinite in water after tilting it for a couple of times.
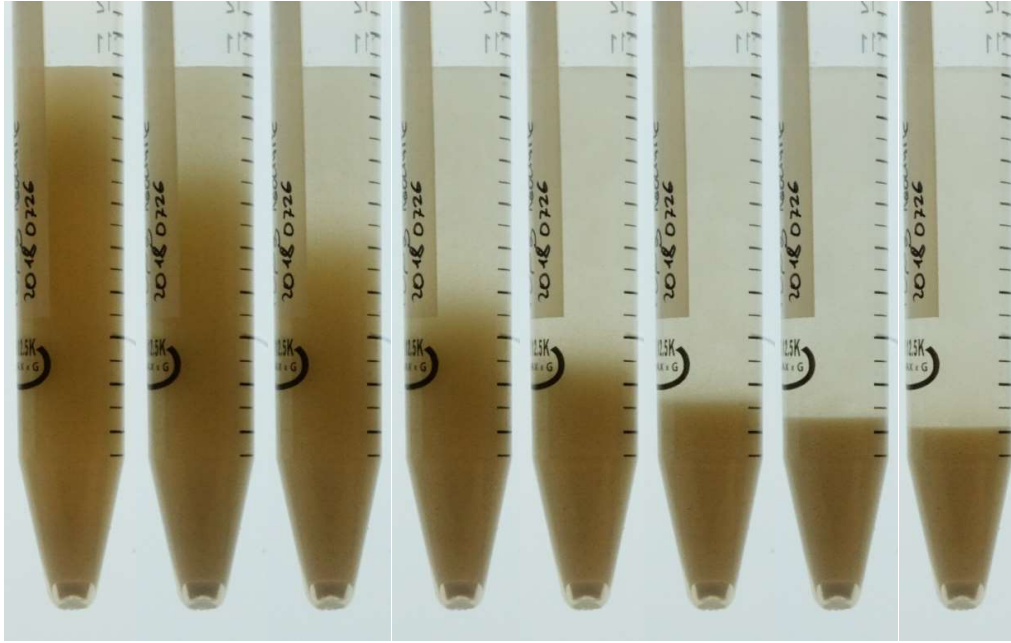
Figure 27: kaolinite in water during the first equilibrium cylcle; each section shows the same vial 15 seconds apart

After approximately two minutes the particles cloud is almost completely settled, during the initial run. However, after doing the equalizing run for a total of four times, the settling speed is significantly slowed down (see Fig. 28). This can be explained by an increase in particle size from clay swelling, which increases the drag thus slowing down the settling.

Figure 28: kaolinite in water after 4 one-hour long equilibrium cycles; each section shows the same vial 15 seconds apart
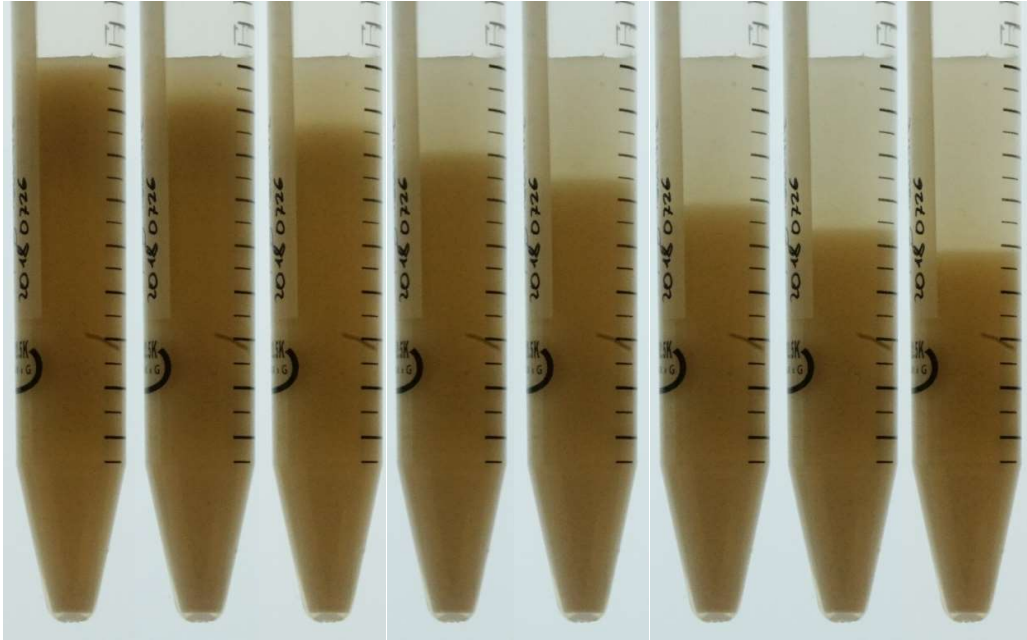
5.2.3 Results

Fig. 29 shows five particle types, each suspended in water, kerosene and a mixture of water and kerosene. The images show the vials after 4 equilibrium runs, in which for example potential swelling has been allowed, and after the final run which has lasted for a few hours.

The final volume of the sediment in all three vials containing silica flour is small compared to the other minerals, because silica flour is quartz sand that does not swell at all. The emulsion in the vial with both water and kerosene is of small volume indicating a weak emulsion that would not withstand a lot of shearing. Volumetric analysis of the emulsion indicates an oil-in-water emulsion which suggests water-wet behavior.

Kaolinite shows higher sediment volumes than silica flour in water due to swelling. In kerosene, the volume is also higher, but this is from the void spaces between agglomerates that form in kerosene as discussed in the sedimentation series. The emulsion is clearly oil-in-water reaching far into the space where pure kerosene used to be at the start of the experiment. Illite behaves similar to kaolinite although the emulsion volume is even larger. Bentonite is extensively expanding in water as evident in the left vial. In the center vial, all water has been transferred into the swollen bentonite paste leaving only kerosene behind. No emulsion formed.

Eagle Ford, which has not penetrated water during the sedimentation test, is not wetted by water even after 4 equilibrium runs. Instead it mostly stays above the surface or sticks to the inside of the vial, which makes it look dirty. In kerosene the color of the organic liquid changes from

transparent to yellow, indicating organic components in the Eagle Ford particles dissolving within the polar liquid phase. The analysis of the polar phase with the GCMS, however did not show any significant changes in the abundance of certain organic compounds. This could be due to the nature of the dissolved organic components. The GCMS here only operates up to 250°C, which is too low to detect components like heavy asphaltenes.

The emulsion that forms in the center vial is mostly occupying former water space, which indicates a water-in-oil emulsion. The extend of the emulsion is not as clear as in the cases with clay minerals due to the dark color of the particles and the unclear transition to the excess Eagle Ford material at the bottom of the vial. Closer examination reveals that there is still free kerosene between the sediment and the emulsion.

Silica Flour after 8 hrs 6min	Kaolinite after 8 hrs 5 min	Illite after 6 hrs 55 min
Bentonite after 6 hrs and 57 min	Eagle Ford after 9 hrs 30 min	
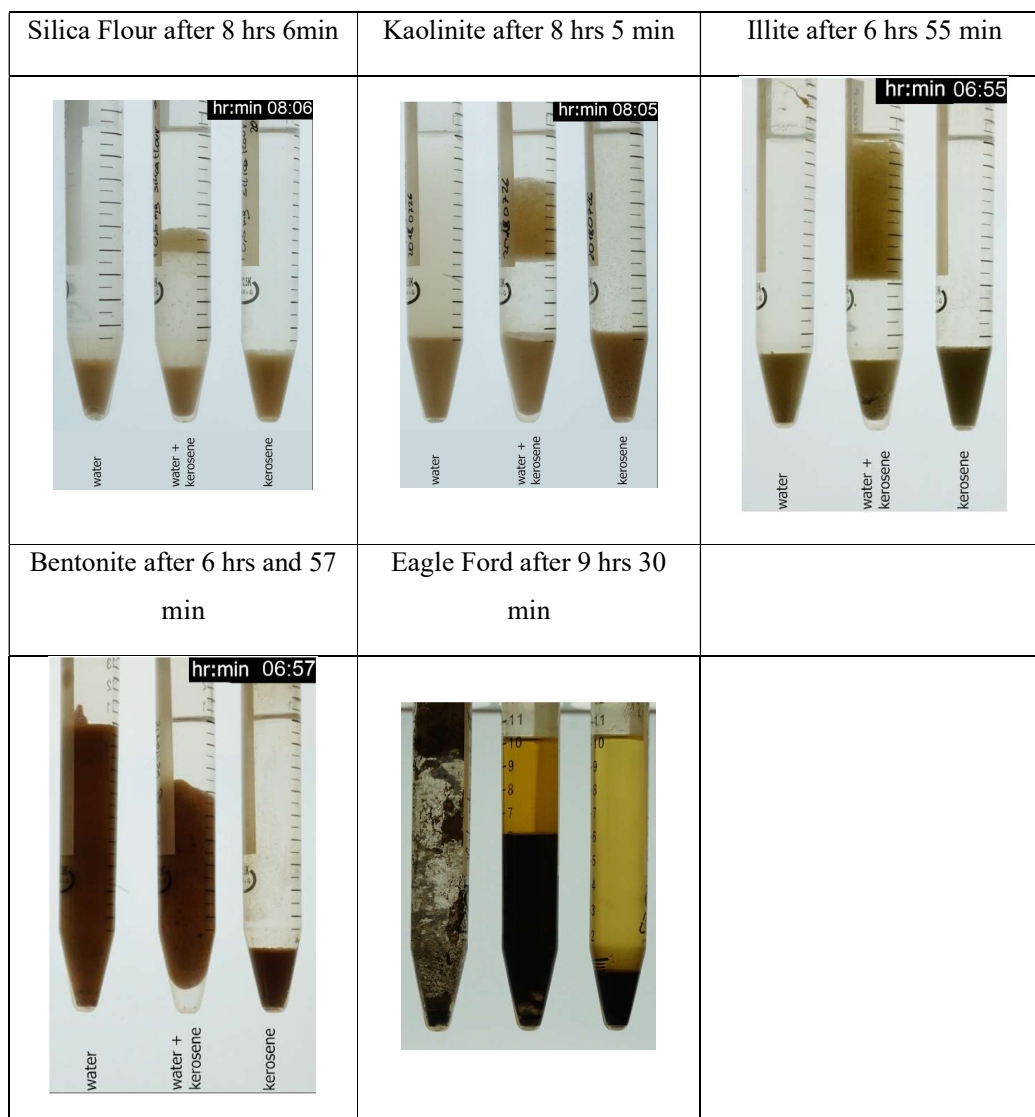
Figure 29: Overview of Emulsion Test on Silica Flour, Kaolinite, Illite, Bentonite and Eagle Ford in water (left image), kerosene (right image) and kerosene-water (center image) after 7 to 10 hours.

5.2.3.1   Effect of the Salinity of the aqueous Phase on the Emulsion

To further understand the effect of salinity on the formation and stability of emulsions, two test runs, one with kaolinite (Fig. 30) and one with silica flour (Fig. 31), each in vials with 5ml of decane and 5 ml of brine with varying NaCl-concentrations, are shown below. Conversely to the experiment with silica flour in water and kerosene, here silica flour in water and decane forms an emulsion. With increasing NaCl concentration however, the emulsion volume diminishes rapidly.

Kaolinite similar to the experiment with kerosene in the previous chapter forms a fairly large and stable emulsion in water and decane. With increasing concentration of NaCl dissolved in water, the emulsion volume decreases initially at 0.1 mol/l. At higher concentrations, the volume of the emulsion increases again almost similar to the water (0 mol/l) case. The structure

of the emulsion however is significantly different, with far less volume of solid incorporated in the emulsion, evident if the sediment volumes are compared. Also, the visible bubbles have a larger diameter for the cases with brine compared to water.
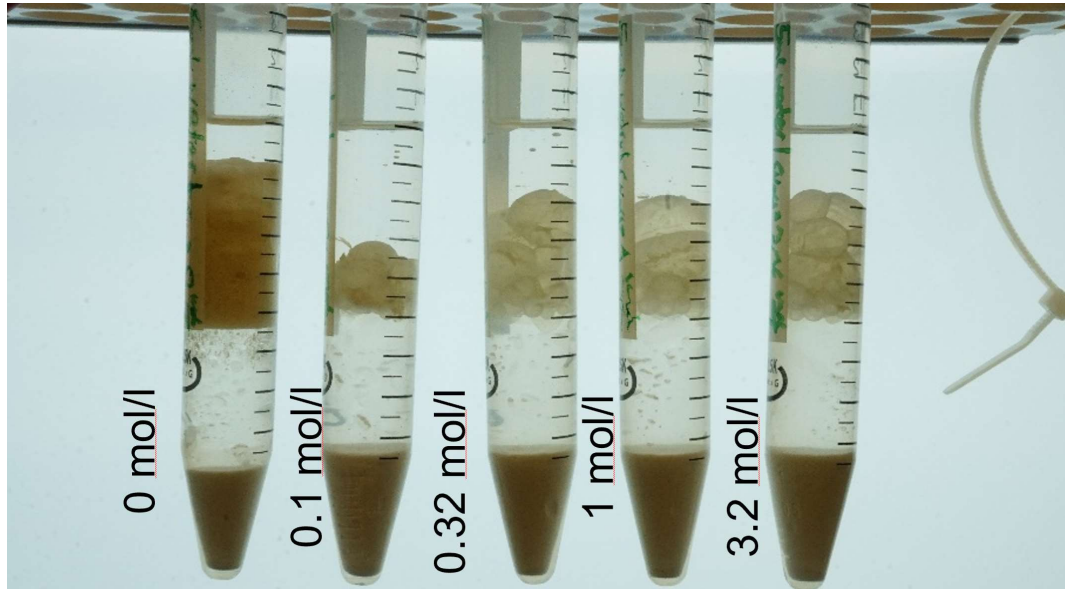
Figure 30: emulsion behavior of kaolinite in 5ml of brine with varying concentrations and 5ml of decane
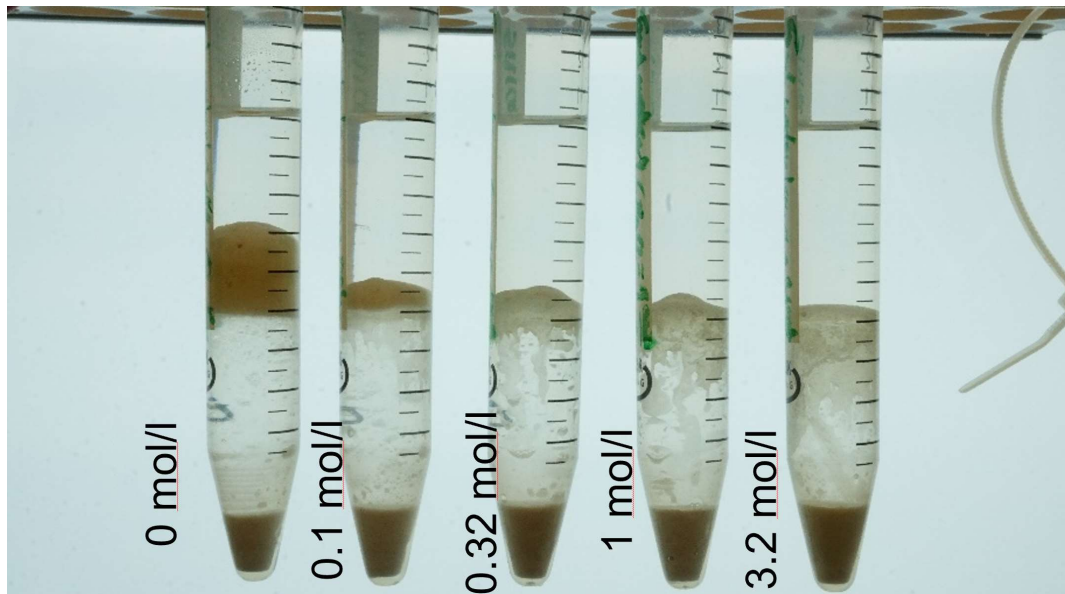
Figure 31: emulsion behavior of silica flour in 5ml of brine with varying concentrations and 5ml of decane

5.2.3.2   Effect of pH of aqueous Phase on the Emulsion

The Fig. 32 below shows kerosene in vials with 5ml of decane and 5ml of an aqueous solution of HCl (pH=3 to pH=6, left vials) and NaOH (pH=8 to pH=11, right vials). The emulsion volumes and structures pictured are all fairly similar, although higher volumes are noticeable for pH values close to 7.

Figure 32: Emulsion Behavior of Kaolinite in 5ml of decane and 5ml of a basic and acidic solution ranging from pH=3 (left vial) to pH=11 (right vial) in steps of one pH value

The emulsion volume is not the only metric to judge the stability of an emulsion. The average bubble size is also frequently used to describe emulsions. Here the bubble size is investigated for pH values ranging from 3 to 7 under the microscope and by manually measuring the bubble features in the software ImageJ:
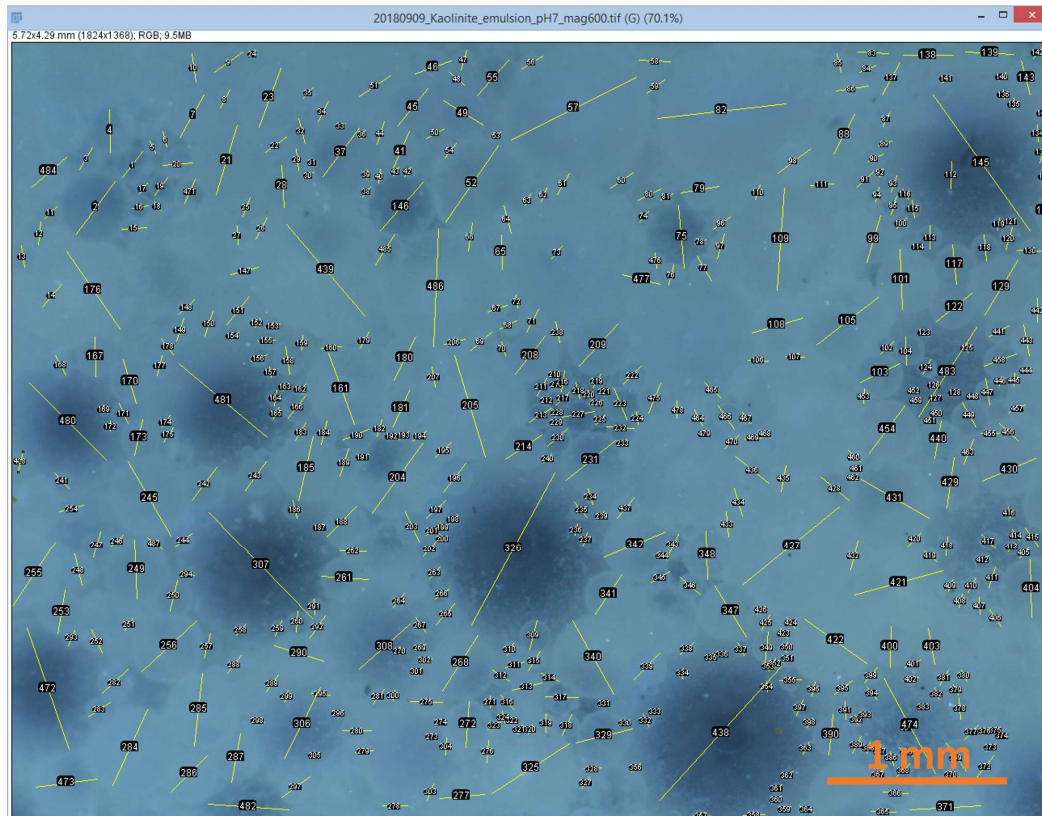
Figure 33: Bubble diameter measurement of a decane-in-HCl (pH=3) emulsion stabilized by Kaolinite particles

The diameter distribution shown as cumulative frequency for pH values 3, 4, 5 and 7 are shown below. The distribution is log-normal and shifts to the right with decreasing pH value. Larger diameters suggest an increase of the contact angle or a change in wettability from the water-wet state towards are more neutral state due to change in the relative position of particle at the fluid interface (see Fig.25). This can be explained by the concept of protonation, thus the change in particle surface charge (see Chapter 3.3.1).
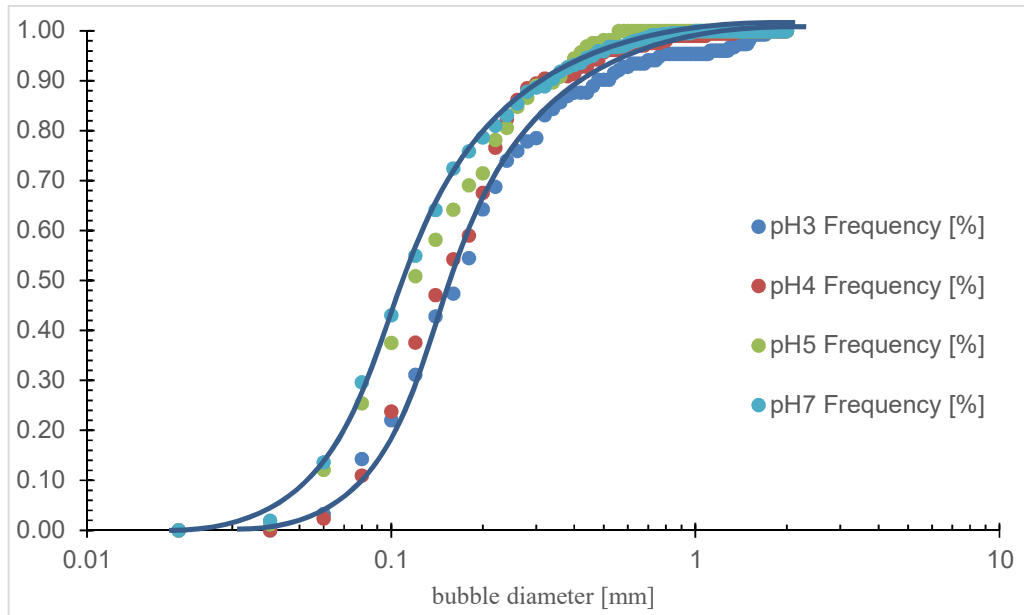
5.2.4 Discussion

Emulsion behavior and type are influenced by the solid type and wettability preference and of course by the liquids that make up the emulsion. Silica flour, kaolinite and illite form oil-in-water emulsions typical for water wet particles. Bentonites swelling capacity can prevent the formation of an emulsion, if the solid absorbs the water phase. Eagle Ford, representing oil-wet particles, forms an oil-in-water emulsion.

Salinity of the water phase influences the structure of the emulsion but does not lead to a wettability reversal from water wet to oil wet. High NaCl-concentrations increase electrostatic repulsion between silica flour particles, which leads to thinning of the foam film. Decane-water emulsions with kaolinite as stabilizers are weak at NaCl-concentrations of 0.1mol/l. The emulsion volume is higher in the test series, because of an increase in the average kerosene bubble diameter suggesting a change of the particle surface charge. The high volume is not synonymous with higher shear resistance, but is nevertheless interesting for practical applications, because less solid material is necessary to form the emulsion compared to a smaller bubble size. The bubble size increases with increasing acidity of the aqueous phase.

Chapter 6

Imbibition Tests

In Chapter 4.1, the behavior of particles at fluid interface has been investigated. The fluids in those experiments are considered static and the particles are moving vertically, driven by gravity and a density difference between the particles and the fluids. Capillary pressure from interfacial tensions either aided in the tendency of particles to move down, for example Silica Flour (water-wet) at the air-water interface or hindered it (e.g.: Eagle Ford at the kerosene-water interface).

To prove that interfacial tension is a driving force, a change of the setup of the sedimentation experiments that eliminates the gravity is proposed. Instead of using a vial, which helps demonstrating vertical movement, a petri dish is used. In the container, powdered rock is saturated with kerosene thus forming a paste, that is distributed equally in the petri dish. After mounting a digital camera above the dish, a 100μl-droplet of a methylene blue and water mixture is placed in the center of the petri dish on top of the powder past using a pipette. By using time lapse photography, the interaction of the droplet with the paste is analyzed qualitatively. For better comparability, a transparent circle is placed on the images digitally.

For some of the experiments desiccation cracks form. They usually occur for drying clays and are a result of capillary forces increasing above the tensional strength of a soil. They are an important in civil engineering and therefore investigated sufficiently by other authors (Shin and Santamarina 2011).

6.1.1 Results

Water readily imbibed into the kerosene-saturated Kaolinite paste. After about 165 min, the droplet that had an initial diameter of around 1 cm, imbibed an area with a diameter of around 3.5 cm. The associated capillary forces cause fines migration and compaction leaving behind desiccation cracks. In Fig. 34 a circular crack around the particle and straight radial cracks outside of the circular crack are predominant. Smaller cracks between the big radial cracks complete a fairly symmetrical end result. The water has "travelled" further than the methylene blue, which adsorbs to the kaolinite.
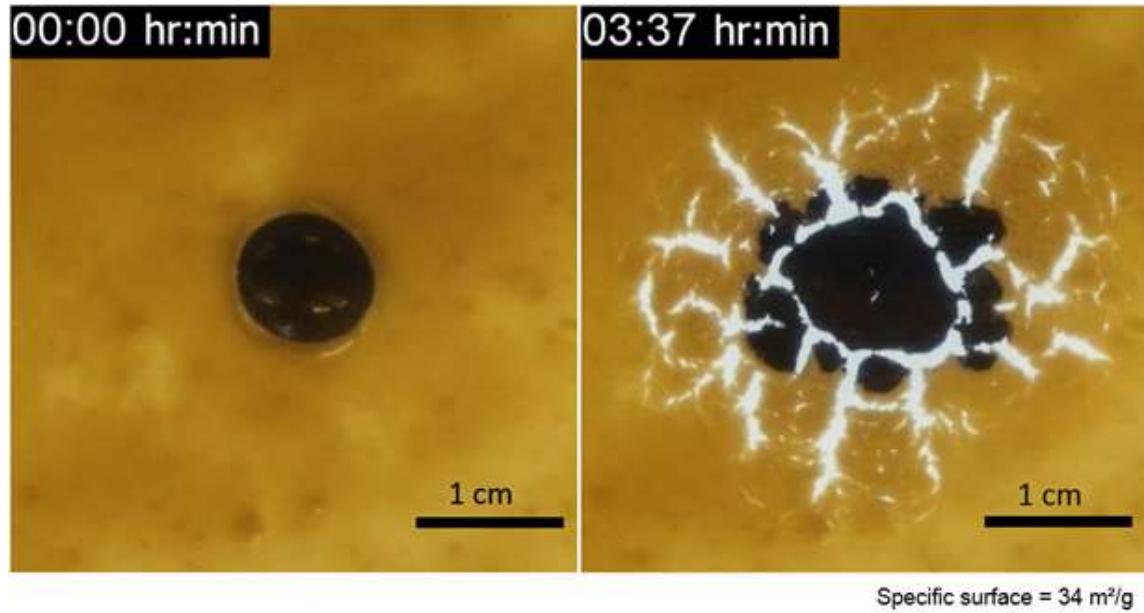
Figure 34: Imbibition of methylene blue and water into kerosene-saturated kaolinite paste

Imbibition into Illite, although reaching an almost similar diameter, takes much longer and has much smaller desiccation cracks. This is because of the higher specific surface area.
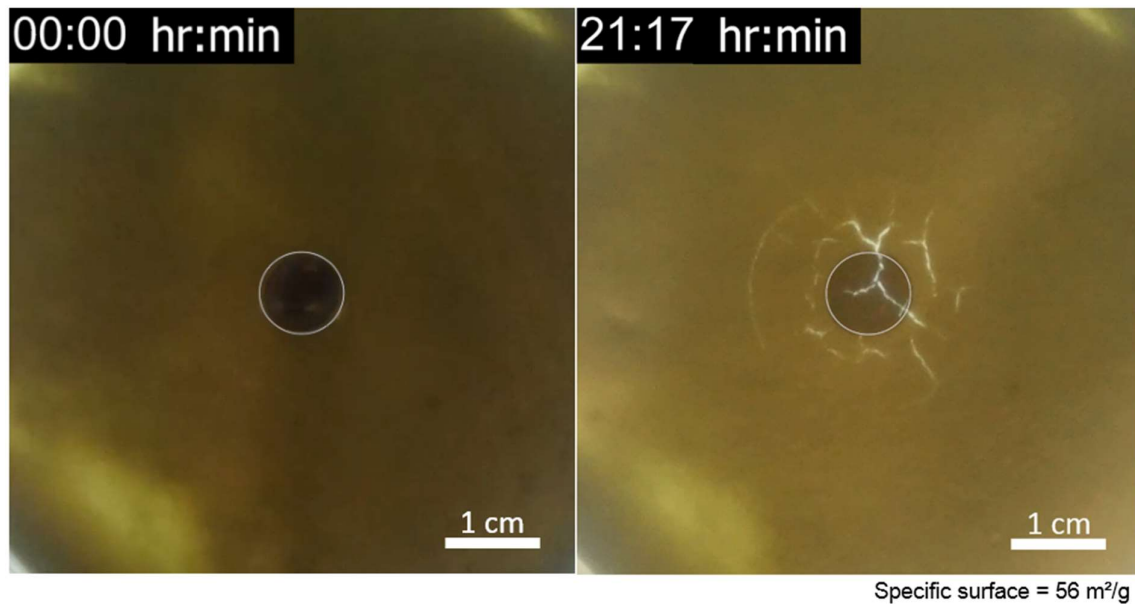
Figure 35: Imbibition of methylene blue and water into kerosene-saturated illite paste

The influence of the surface area on the imbibition becomes evident for bentonite, which has a significantly higher specific surface compared to silica flour and kaolinite. For bentonite, the influenced are only has a diameter of around 1.3 cm. The desiccation crack is almost completely circular and is formed solely by an inward movement of the contracting inner area.
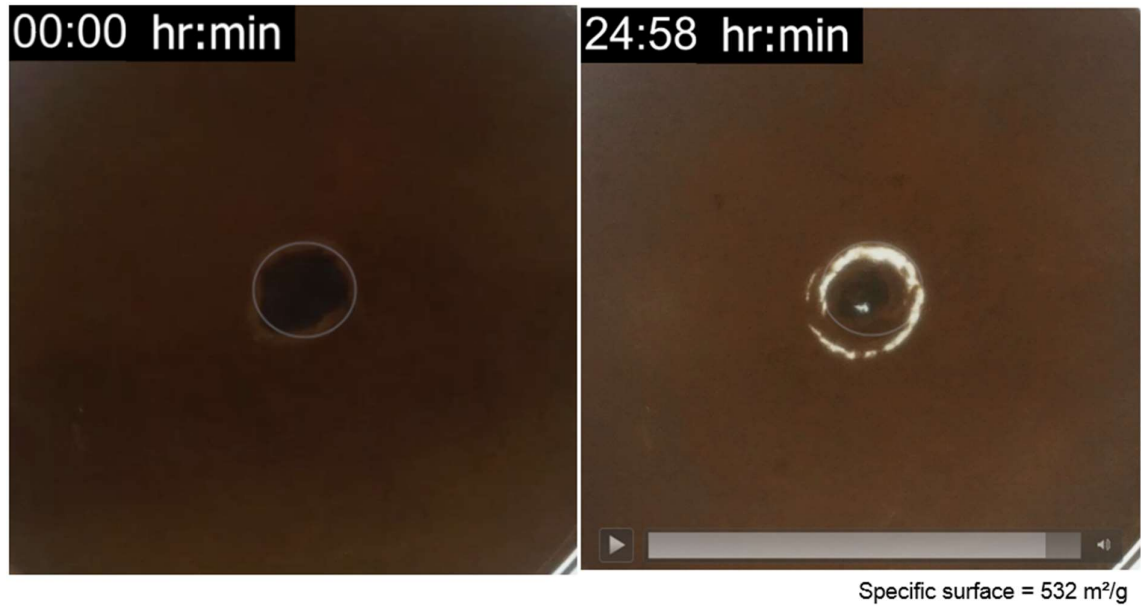
Figure 36: Imbibition of methylene blue and water into kerosene-saturated bentonite paste

Water imbibition into Silica Flour paste has been significantly slower than with kaolinite, but the affected area is larger than that of kaolinite. Methylene blue travels almost as far as water, because the specific surface area of Silica Flour is extremely low, which mitigates adsorption of molecules to the particles. The circular features like the area imbibed by methylene blue that appeared for the clay minerals, are not present.
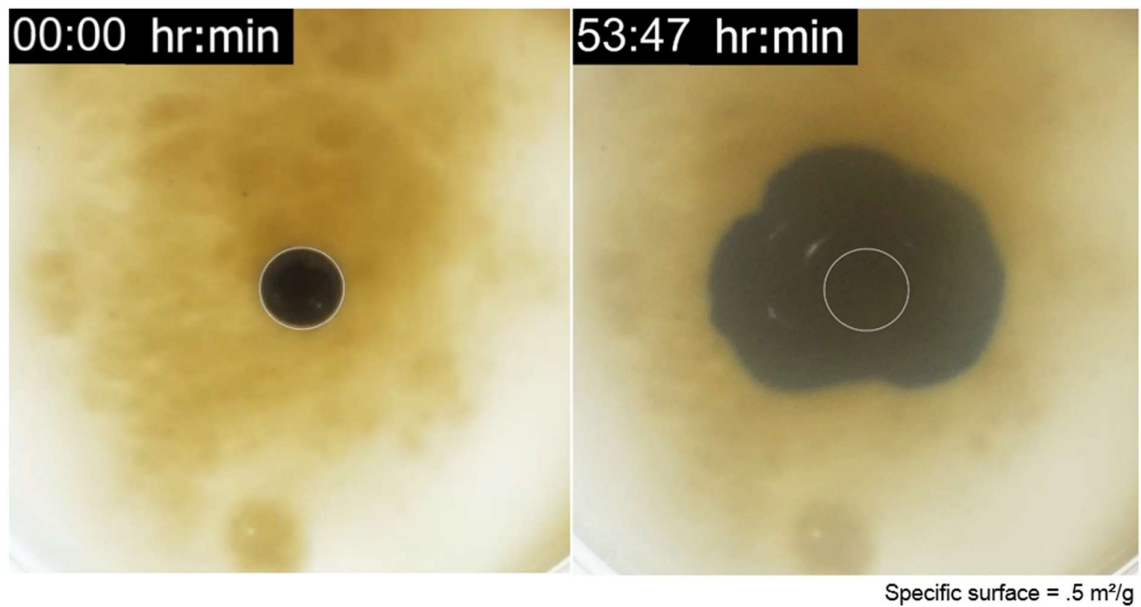
Figure 37: Imbibition of methylene blue and water into kerosene-saturated silica flour paste

Water did not imbibe into the kerosene-saturated Eagle Ford paste. The droplet stays on top of the kerosene paste with almost no visible imbibition. This matches the observations made

during the sedimentation test. The oil wet Eagle Ford rock did not penetrate the air ware interface.

6.1.2 Summary and Discussion

Instantaneous imbibition of water into a kerosene-saturated rock particle paste is affected by the wettability of the particle and its specific surface. For the clay minerals, the specific surface increases from kaolinite over illite to bentonite. In the same sequence, the imbibition time increases and the affected imbibition area decreases. The effect of specific surface becomes even more obvious by looking at the travel distance of methylene blue, which is very large for illite and basically non-existent for bentonite.

Silica flour and the clay minerals are water wet, which has allowed imbibition of water. The oil wet Eagle For on the other hand has not allowed spontaneous imbibition of water, because of the contact angle of water and kerosene on the rock particles. Force would be necessary to overcome the capillary pressure.

	Silica Flour	Kaolinite	Illite	Bentonite	Eagle Ford
Specific Surface [m^2/g]	0.5	34	56	532	
Imbibition completion time [hrs:min]	17:00	2:45	14:00	n/a	t→inf
Imbibition circle diameter [cm]	4.6	3.5	2.9	1.3	1

Chapter 7

Conclusion

Raining powdered rock on polar and non-polar liquid interface provides insightful information on rock-liquid interactions. Wettability, density of solids and fluids and particle size influence whether particles stay at fluid interfaces or sink. Water-wet Silica flour, kaolinite and illite minerals sink into water at an air-water interface. Oil-wet Eagle Ford does not sink at the same interface due to the unfavorable contact angle. At the air kerosene interface all minerals, independent of their affinity for water or oil sink, because of the lowered interfacial tension of the liquid phase. At the kerosene-water interface kaolinite and silica flour exhibit a non-zero residence time. Illite, bentonite and Eagle Ford are not heavy enough to sink.

Pickering emulsions are emulsions stabilized by solid particles. All mineral types tested have been able to form stable emulsions. Behavior and type of the emulsion is influenced by the solid type and wettability preference and of course by the liquids that make up the emulsion. Silica flour, kaolinite and illite form oil-in-water emulsions, typical for water wet particles. Bentonites swelling capacity can prevent the formation of an emulsion, if the solid absorbs the water phase. Eagle Ford, representing oil-wet particles, forms an oil-in-water emulsion. Salinity of the water phase influences the structure of the emulsion but does not lead to a wettability reversal from water wet to oil wet. High NaCl-concentrations increase electrostatic repulsion between silica flour particles, which leads to thinning of the foam film. Decane-water emulsions with kaolinite as stabilizers are weak at NaCl-concentrations of 0.1mol/l. Higher salinities increase the emulsion volume but decrease the particle association of the clay radically changing the structure of the emulsion.

The bubble size increases with increasing acidity of the aqueous phase. The bubble size depends on the relative vertical position of a particle or the relative surface touching the two fluid interfaces and depends (apart from other things) on the contact angle on the particle. Protonation of the particle (Chapter 3.3.1) increases the surface charge changing the size of the double layer and therefore the wettability of the particle. Here, a change in wettability from water-wet towards a more neutral wet state is suggested.

Imbibition tests are a different type of interface behavior test, but instead of the solids moving by gravitational force like in the sedimentation test series, water travels through the solid pores displacing kerosene by capillary force. Instantaneous imbibition of water into a kerosene-saturated rock particle paste is affected by the wettability of the particle and its specific surface. Specific surface decreases travel distance and speed. Non-favorable wetting conditions can hinder spontaneous imbibition, for example in the case of oil-wet Eagle Ford which is not imbibed spontaneously by water.

7.1   Technical Limitations

The following chapter is intended to recap on aspects that could have been done differently and shall be a guide for future tests, following this this thesis.

7.1.1   Emulsion Preparation

7.1.1.1   Mixing Sequence

With the established procedure described in Chapter 4.3.1, the preparation of the emulsion can be considered uncareful. The vials have been filled with water or brine first, followed by kerosene or decane depending on the test series. The powder has been added as the last step by pouring it on top of the hydrocarbon layer.

In the description of emulsion preparations done in similar research papers, it is suggested to extensively mix the solids with the water or brine phase before adding the hydrocarbon phase to form oil-in-water emulsions (Chevalier and Bolzinger 2013). Although wettability alteration is mostly attributed to heavy hydrocarbon components like asphaltenes (see Chapter 1.3.2), the influence of some of the heavy components or impurities especially in the customary kerosene cannot be neglected and probably altered the outcome of some of the experiments.

7.1.1.2   Mixing energy

In the same paper Chevalier and Bolzinger also mention how to properly mix the emulsion. They use an Ultra-Turray rotor stator device rotating with 10000 to 20000 rpm for ten minutes. This is far more mixing energy than in the experimental setup (Chapter 3 and 4). Vigorous mixing leads to a better distribution of the solid particles and a smaller droplet size of the dispersed phase.

7.1.1.3   Solid Content

In some papers, the treatment of quartz particles with HCL to remove impurities like ferric ions are mentioned (Fuerstenau, Diao et al. 1991) and (Dubey and Doe 1993). Higher contents of solids tend to neutralize the pH of the liquid it is suspended in (Palomino, Santamarina et al. 2005). Subsequent measurements and corrections of the pH value are necessary to guarantee applicable results.

In some papers, the treatment of particles with trymethylchlormethane is proposed (Fuerstenau, Diao et al. 1991). Sufficient TMCS makes the solid surface homogeneously homophobic.

7.1.2   Container Material

After two to three days, deformation of the vials partly (5ml) or solely (10ml) filled with kerosene in form of bending of the vial was apparent. Some interaction between the kerosene and the plastic material must have occurred, because similar vials filled with water or brine did not show any deformation.

The vial material was slightly hydrophobic, which led to a contact angle higher than 90° in the experiments involving both polar and non-polar fluids evident in the meniscus pointing upwards (see Fig. 38 (a)). The interface shape brings up several issues. The particles initially poured into the vials do not spread equally on the liquid interface. Instead they slide or roll down the curved interface and accumulate close to the vials surface in form of a wedge. While the particle transmission in the center of the vial seem fairly uniform, the behavior close to the vial surface is sometimes irregular with small aggregations of particles sticking longer this position than the particles in the center (see Fig. 38 (b)). Additionally, the curved nature of the interface turns out to be an issue in image capturing. Without the powdered material, the interface seems quite well defined (see Fig. 38). After the sedimentation test series, particles are attached to the interface, making it harder to decide at which point the sedimentation is complete. This leads to imprecise comparisons between the different experiments conducted.
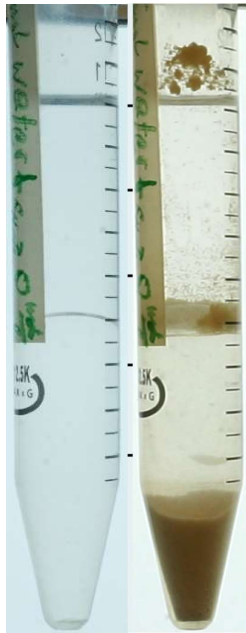
Figure 38: (a) Test vial filled with 5ml of water (bottom) and 5ml of kerosene (top) and the same test vial appr. 5 min. after starting the sedimentation test

The petri dishes used during the imbibition test series have been closed with the appropriate cover, which does not seal the inside completely. Kerosene is very volatile and thus escaped particularly for those experiments that took longer than a day.

Appendix A

Appendix

7.2   List of References

Adamson, A. W. and A. P. Gast (1967). Physical chemistry of surfaces, Interscience New York.

Afrapoli, M. S., et al. (2009). "The effect of bacterial solution on the wettability index and residual oil saturation in sandstone." **69**(3-4): 255-260.

Ahmed, U. and D. N. Meehan (2016). Unconventional oil and gas resources: exploitation and development, CRC Press.

Allen, T. (2013). Particle size measurement, Springer.

Amott, E. (1959). "Observations relating to the wettability of porous rock."

Anderson, W. G. J. J. o. p. t. (1986). "Wettability literature survey-part 1: rock/oil/brine interactions and the effects of core handling on wettability." **38**(10): 1,125-121,144.

Aveyard, R., et al. (2003). "Emulsions stabilised solely by colloidal particles." Advances in Colloid and Interface Science **100**: 503-546.

Binks, B. P. and T. S. Horozov (2006). Colloidal particles at liquid interfaces, Cambridge University Press.

Buckley, J. and N. Morrow (1990). Characterization of crude oil wetting behavior by adhesion tests. SPE/DOE Enhanced Oil Recovery Symposium, Society of Petroleum Engineers.

Chevalier, Y. and M.-A. Bolzinger (2013). "Emulsions stabilized with solid nanoparticles: Pickering emulsions." Colloids and Surfaces A: Physicochemical and Engineering Aspects **439**: 23-34.

Cuss, R. J., et al. (2011). "Fracture transmissivity as a function of normal and shear stress: first results in Opalinus Clay." Physics and Chemistry of the Earth, Parts A/B/C **36**(17-18): 1960-1971.

de Laplace, P. S. (1807). Supplément à la théorie de l'action capillaire.

Deraguin, B. and L. J. A. P. U. Landau (1941). "Theory of the stability of strongly charged lyophobic sols and of the adhesion of strongly charged particles in solution of electrolytes." **14**: 633-662.

Donaldson, E. C., et al. (1969). "Wettability determination and its effect on recovery efficiency." Society of Petroleum Engineers Journal **9**(01): 13-20.

Dubey, S. and P. Doe (1993). "Base number and wetting properties of crude oils." SPE Reservoir Engineering **8**(03): 195-200.

Dubey, S. and M. J. S. R. E. Waxman (1991). "Asphaltene adsorption and desorption from mineral surfaces." **6**(03): 389-395.

Dymond, J., et al. (1994). "Viscosity of selected liquid n-alkanes." **23**(1): 41-53.

Frelichowska, J., et al. (2010). "Effects of solid particle content on properties of o/w Pickering emulsions." Journal of colloid and interface science **351**(2): 348-356.

Fuerstenau, D., et al. (1991). "Characterization of the wettability of solid particles by film flotation 1. Experimental investigation." Colloids and Surfaces **60**: 127-144.

Garbsva, S., et al. (1978). "Hydrophobic characterization of powder Some criteria and experimental evidence." **256**(3): 241-250.

Guibet, J. and E. J. E. T. Faure-Birchem, Paris (1999). "Fuels and Engines, vol. 1."

Gutierrez, M., et al. (2000). "Stress-dependent permeability of a de-mineralised fracture in shale." Marine and Petroleum Geology **17**(8): 895-907.

Hamaker, H. C. J. p. (1937). "The London—van der Waals attraction between spherical particles." **4**(10): 1058-1072.

Hayes, R. A., et al. (1993). "Forced liquid movement on low energy surfaces." **159**(2): 429-438.

Hirasaki, G. J. S. F. E. (1991). "Wettability: fundamentals and surface forces." **6**(02): 217-226.

Israelachvili, J. N. (2011). Intermolecular and surface forces, Academic press.

Kolarov, T., et al. (1990). "Profile of the transition region between aqueous wetting films on quartz and the adjacent meniscus." **51**: 37-47.

Kralchevsky, P., et al. (2005). "On the thermodynamics of particle-stabilized emulsions: curvature effects and catastrophic phase inversion." Langmuir **21**(1): 50-63.

Kralchevsky, P. and K. Nagayama (2001). Particles at fluid interfaces and membranes: attachment of colloid particles and proteins to interfaces and formation of two-dimensional arrays, Elsevier.

Lyklema, J. (2005). Fundamentals of interface and colloid science, Volume IV, Chapter 3, Elsevier/Academic Press, Amsterdam.

Morrow, N. R. (1990). "Wettability and its effect on oil recovery." Journal of petroleum technology **42**(12): 1,476-471,484.

Palomino, A. M. (2003). Fabric formation and control in fine-grained materials, Georgia Institute of Technology.

Palomino, A. M., et al. (2008). "Mixtures of fine-grained minerals–kaolinite and carbonate grains." **56**(6): 599-611.

Palomino, A. M., et al. (2005). "Fabric map for kaolinite: effects of pH and ionic concentration on behavior." **53**(3): 211-223.

Peters, K. E., et al. (2005). The biomarker guide, Cambridge University Press.

Pickering, S. U. J. J. o. t. C. S., Transactions (1907). "Cxcvi.—emulsions." **91**: 2001-2021.

Ramsden, W. J. P. o. t. r. S. o. L. (1903). "Separation of solids in the surface-layers of solutions and'suspensions'(observations on surface-membranes, bubbles, emulsions, and mechanical coagulation).--preliminary account." **72**: 156-164.

Santamarina, J., et al. (2002). "Micro-scale aspects of chemical-mechanical coupling: Interparticle forces and fabric." Chemical Behaviour: Chemo-Mechanical Coupling from Nano-Structure to Engineering Applications: 47-64.

Santamarina, J. C., et al. (2001). "Soils and waves: Particulate materials behavior, characterization and process monitoring." **1**(2): 130-130.

Shin, H. and J. J. G. Santamarina (2011). "Desiccation cracks in saturated fine-grained soils: particle-level phenomena and effective-stress analysis." **61**(11): 961.

Sposito, G. J. E. s. t. (1998). "On points of zero charge." **32**(19): 2815-2819.

Verwey, E. J. W. J. T. J. o. P. C. (1947). "Theory of the stability of lyophobic colloids." **51**(3): 631-636.

Young, T. (1855). Miscellaneous works of the late Thomas Young, J. Murray.

Zeppieri, S., et al. (2001). "Interfacial tension of alkane+ water systems." **46**(5): 1086-1088.

7.3   Summary of common Wettability Test Methods

7.3.1 Adhesion Tests

Adhesion tests can be conducted to characterize the interaction of crude oil with reservoir minerals (Buckley and Morrow 1990). Flat and smooth mineral surfaces overlain by brine are contacted by a droplet of crude for 2 minutes, which is then withdrawn. Fig 39. shows the two possible outcomes of the simple experiment: Either the droplet attaches to the mineral surface or is removed during the withdrawal of the transportation syringe. This depends on the stability of the thin brine film between oil droplet and solid surface. If the sign of the surface charge of the solid/brine interface and the charge at the brine/oil interface are the same and the magnitude is high enough, the brine system can maintain stable and thus hinder attachment of the oil droplet on the mineral surface.
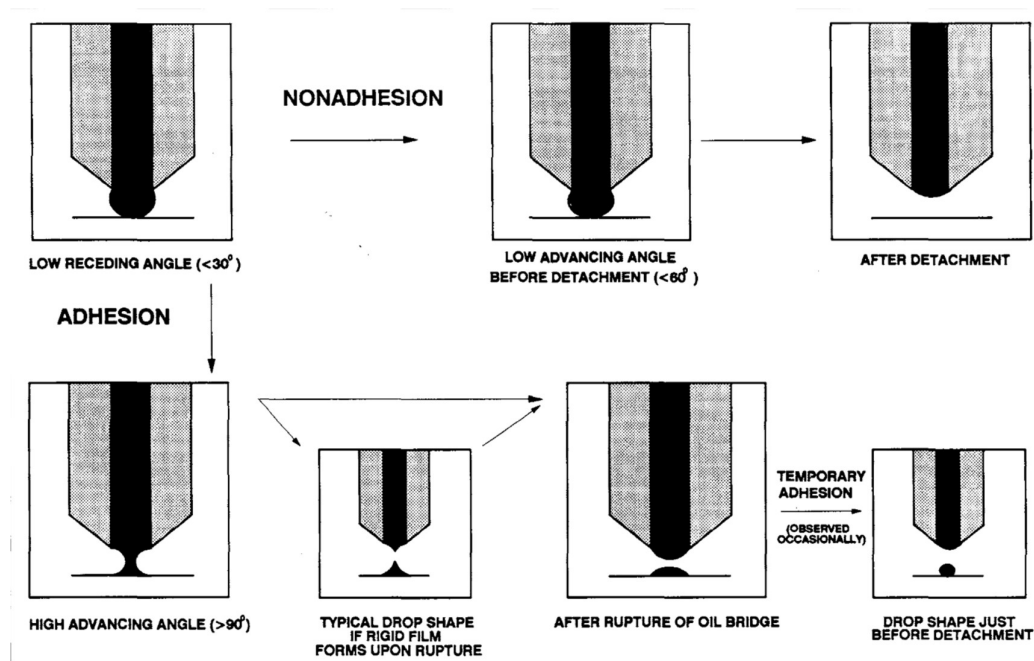

Figure 39: Adhesion test of crude oil (Morrow 1990)

Apart from the typical difficulties for simple wettability tests mentioned at the beginning of the chapter, this test method is also strongly influenced by gravity. Additionally, the charges at the

interfaces are a function of pH and adhesion of the droplet is especially sensitive to changes in pH close to neutral.

7.3.2 Amott Test

The Amott test (Amott 1959) measures wettability of a porous rock as a function of the displacement properties of oil and water within the rock.

It uses funnel shaped tubes out of Lucite during water displacement and glass during oil displacement, in which cores from the investigated rocks are mounted. Testing of unconsolidated sand is possible by using a Lucite cover. The size of the core ranges from 0.75" to 1" in diameter and 1" to 3" in length.

Procedure:

1. Flush core with water and with kerosene to remove most of the crude oil and formation water.
2. Evacuate under kerosene to remove gas.
3. Centrifuge under water to obtain core at residual oil saturation (1800g for 1 hour).
4. Blot core and immerse in kerosene. Record volume of water spontaneously released after 20 hours.
5. Centrifuge under kerosene and record total volume of water displaced (1800g for 1 hour).
6. Blot core and immerse in water. Record volume of oil spontaneously released after 20 hours.
7. Centrifuge under water and record total volume of oil displaced.

Originally, the ratio of spontaneous displacement vs. total displacement volumes have been used as wettability indices. As an example, a displacement-by-water-ratio of 1 and a displacement-by-oil-ratio of 0 would suggest a strongly water wet rock core.

$$I_w = \frac{\text{displaced oil from imbibition of water}}{\text{total oil displaced from spontaneous and forced imbibition of water}}$$

$$I_o = \frac{\text{displaced water from imbibition of oil}}{\text{total wate displaced from spontaneous and forced imbibition of oil}}$$

This system with two values ranging from 0 to 1 has since then been combined into a single value called the Amott-Harvey-Index, that is the subtraction of the displacement ratios of water and oil: $I_{AH} = I_w - I_o$. It ranges from -1 (strongly oil wet) to +1 (strongly water wet).

To avoid changes in wettability during testing, drastic core handling procedures should be avoided (no extracting, drying, etc.).
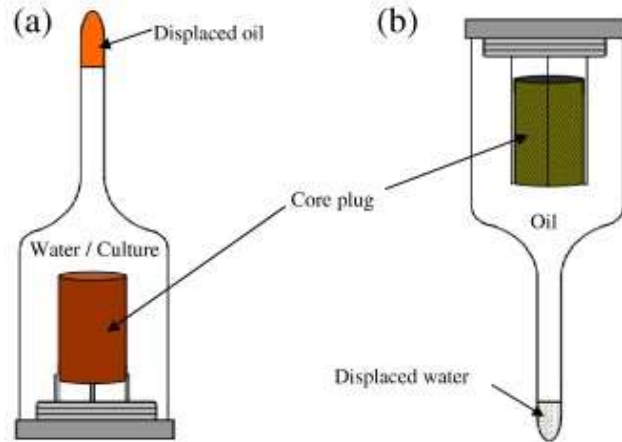
Figure 40: Amott test setup (Afrapoli, Crescente et al. 2009)

7.3.3 USBM Test

The USBM test (Donaldson, Thomas et al. 1969) is similar to the Amott test. Cores are placed inside a centrifuge, but instead of applying constant forces for a certain time span, incremental speeds of the centrifuge are used. The equivalent capillary pressure is measured and plotted against the water saturation of the core.

- Crude oil instead of kerosene.
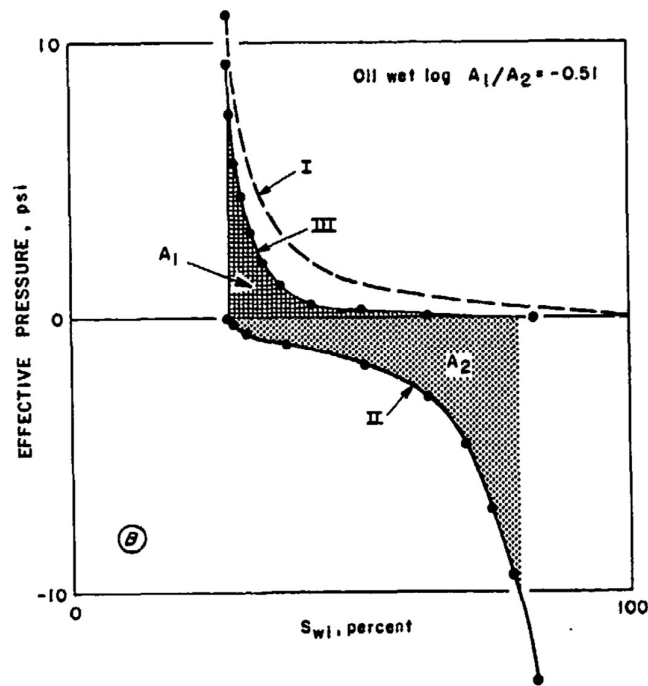- The logarithm of the ratio of the areas under the curves define wettability.

Figure 41: Capillary pressure curve of an oil wet core sample (Donaldson, Thomas et al. 1969)

Procedure:

- Core samples of 3.3cm length and 1.9cm diameter are saturated with brine (0.1N sodium chloride) under vacuum.
- Core placed in holder with 2ml-collecting section designed to fit the original centrifuge buckets. Core holder is filled with oil and centrifuged at 2300gm until no more brine is displaced. ->residual water saturation + initial oil saturation
- Core placed in another core holder filled with brine, inverted and centrifuged at incremental speeds to 2300 gm. From amount of oil displaced at each constant speed, measured with a stroboscope, capillary pressure curve II was obtained.
- Core placed in oil and the volume of brine displaced at incremental speed increases is measured. -> capillary pressure curve.

7.3.4 Film Flotation

Film Flotation (Fuerstenau, 1991) is a method to get the critical wetting surface tension of particles by measuring the percentage of particles that float as a function of the surface tension of an aqueous methanol solution. The surface tensions is changed by changing the ratio of water and methanol in the solution.
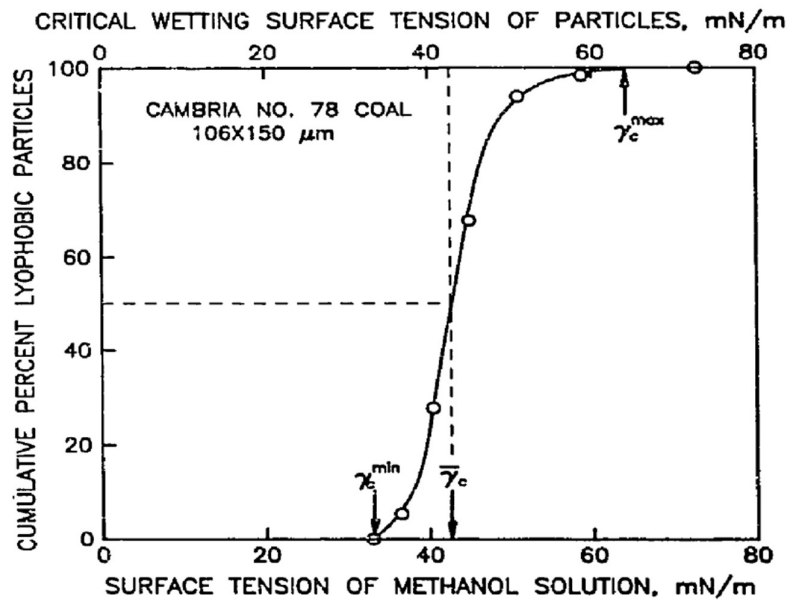

Figure 42: The cumulative percentage of hydrophobic particles as a function of wetting surface tension in film flotation tests

Procedure:

- 0.2g-0.3g of closely sized particles (106x150 microns) onto surface of the liquid (aqueous methanol solutions) in a single container (radius=5cm, depth=1cm, conical bottom with stopcock on the drain)
- Depending on wetting characteristics of the material and the surface tension of the liquid used, the particles either remain at the liquid vapor interface or are immediately engulfed by the liquid and subsequently sink.
- In the absence of gravitational effects, a particle transfers spontaneously from the interface into the liquid phase just when the contact angle becomes zero, that is when

the fil of liquid can spread over the entire particle. Therefore, at any point along the curve in Fig. 42, the particles that sink have their individual values of the critical surface tensions that are equal to the surface tensions of the wetting liquid used in the film flotation.

- Histogram of weight percent vs. critical surface tension is plotted to show average critical wetting surface tension of particles and standard deviation (=heterogeneity)
- Particle size, particle density, particle shape, film flotation time and the nature of the wetting liquid were found to have a negligible effect on the results of film flotation in the ranges tested. Film flotation is sensitive mainly to the surface hydrophobicity and heterogeneity of particles.
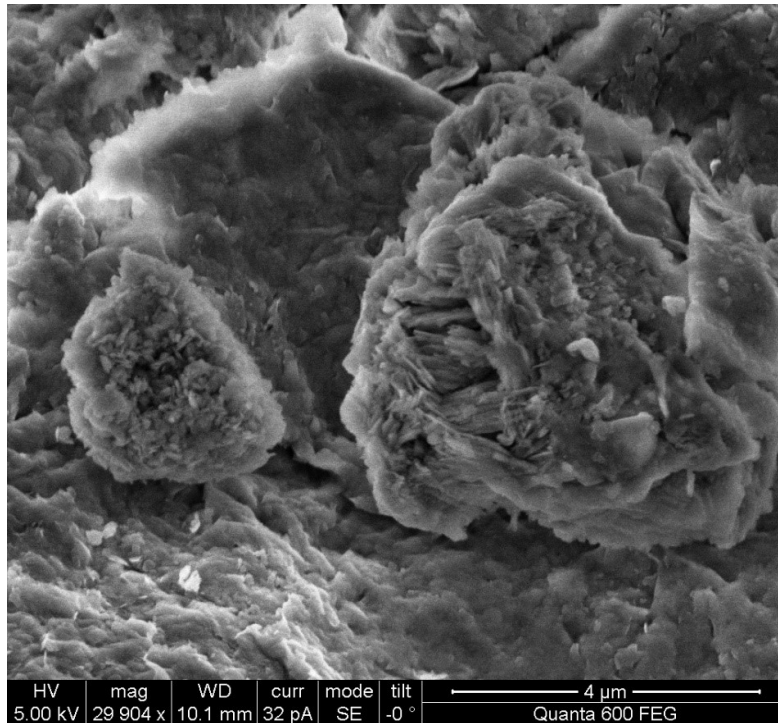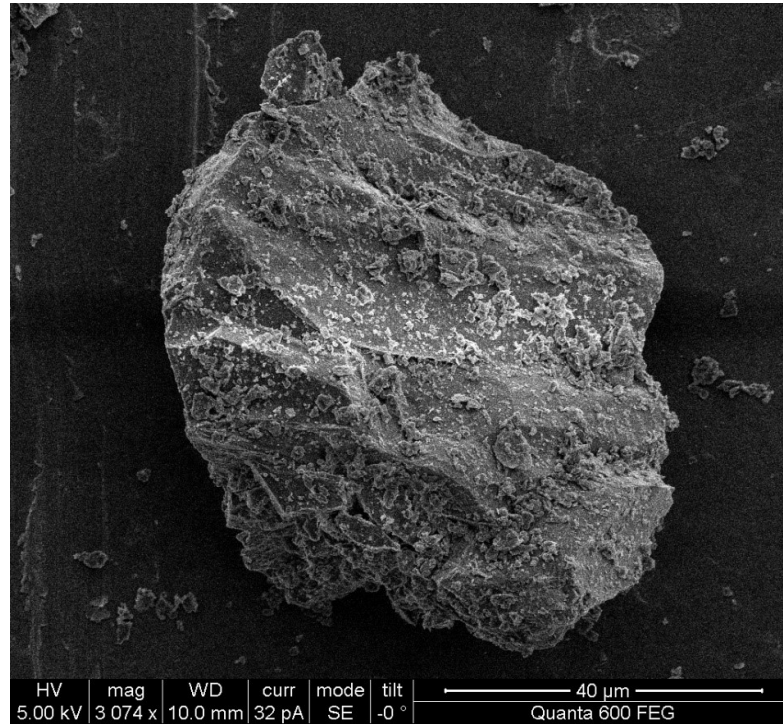
7.4   SEM images

Figure 43: SEM image of Bentonite

Figure 44: SEM image of Silica Flour

7.5   Derivation of the Force Balance Equation of a Particle at an oil-water interface

The following equation is called Equ. (10) in Chapt.

$$-\gamma_{ow} \cdot 2\pi r \sin \Phi_c \sin(\Phi_c + \theta) + \rho_w \frac{r^3 \pi}{3}(2 - 3\cos \Phi_c + \cos^3 \Phi_c)g$$

$$+ \rho_o \left(\frac{4r^3 \pi}{3} - \frac{r^3 \pi}{3}(2 - 3\cos \Phi_c + \cos^3 \Phi_c) \right)g$$

$$- (\rho_w - \rho_o)gz_c(r \cdot \sin \Phi_c)^2\pi = \rho_p \frac{4r^3 \pi}{3}g$$

Rearrangement, so that only $\sin \Phi_c \sin(\Phi_c + \theta)$ is on the left side of the equation, necessary for the interpretation

$$\sin \Phi_c \sin(\Phi_c + \theta)$$

$$= \frac{1}{-\gamma_{ow} \cdot 2\pi r} \left[\rho_p \frac{4r^3 \pi}{3}g - \rho_w \frac{r^3 \pi}{3}(2 - 3\cos \Phi_c + \cos^3 \Phi_c)g \right.$$

$$- \rho_o \left(\frac{4r^3 \pi}{3} - \frac{r^3 \pi}{3}(2 - 3\cos \Phi_c + \cos^3 \Phi_c) \right)g$$

$$\left. + (\rho_w - \rho_o)gz_c(r \cdot \sin \Phi_c)^2\pi \right]$$

Reduce r and π-components in the fractions, factor numbers and g outside the brackets and rearrange some signs:

$$\sin \Phi_c \sin(\Phi_c + \theta)$$

$$= -\frac{r^2 g}{\gamma_{ow} \cdot 6} \left[\rho_p 4 - \rho_w(2 - 3\cos \Phi_c + \cos^3 \Phi_c) \right.$$

$$\left. - \rho_o(2 + 3\cos \Phi_c - \cos^3 \Phi_c) - 4\rho_o + 3(\rho_w - \rho_o)\frac{z_c}{r}(\sin \Phi_c)^2 \right]$$

$$= -\frac{r^2 g}{\gamma_{ow} \cdot 6} \left[\rho_p 4 - (\rho_w - \rho_o)(-2 - 3\cos \Phi_c + \cos^3 \Phi_c) - 4\rho_o \right.$$

$$\left. + 3(\rho_w - \rho_o)\frac{z_c}{r}(\sin \Phi_c)^2 \right]$$

Factoring of $p_w - p_o$:

$$\sin \Phi_c \sin(\Phi_c + \theta)$$

$$= -\frac{(\rho_w - \rho_o)r^2 g}{\gamma_{ow} \cdot 6} \left[4\frac{\rho_p - \rho_o}{(\rho_w - \rho_o)} - (-2 - 3\cos \Phi_c + \cos^3 \Phi_c) \right.$$

$$\left. + 3\frac{z_c}{r}(\sin \Phi_c)^2 \right]$$

The middle term in the square brackets can be divided into two factors:

$$\sin \Phi_c \sin(\Phi_c + \theta)$$

$$= -\frac{(\rho_w - \rho_o)r^2 g}{\gamma_{ow} \cdot 6}\left[4\frac{\rho_p - \rho_o}{\rho_w - \rho_o} - (1 - \cos^2 \Phi_c)(2 - \cos \Phi_c)\right.$$

$$\left. + 3\frac{z_c}{r}(\sin \Phi_c)^2\right]$$

In the final step, the Bond number is introduced.

$$B = \frac{(\rho_w - \rho_o)r^2 g}{\gamma_{ow}}$$

$$\sin \Phi_c \sin(\Phi_c + \theta) = -\frac{B}{6}\left[4\frac{\rho_p - \rho_o}{\rho_w - \rho_o} - (1 - \cos^2 \Phi_c)(2 - \cos \Phi_c) + 3\frac{z_c}{r}(\sin \Phi_c)^2\right]$$

7.6   Materials

7.6.1 Solids

The silica flour was bought from BMS factories (Jeddah, Saudi-Arabia). It is specified as 95% pure SiO2 with a specific gravity of 2.65 and 75 microns in diameter. The quartz sand is used as a counterpart to the clay particles, which does not swell but is water wet.

The Kaolinite was obtained from Wilkinson Kaolin Associates (Gordon, Georgia, USA). The manufacturer specifies values for specific gravity of 2.6 and an approximate diameter $d_{50} = 1.1\mu m$ of the hexagonal particle. Measurements done on the SEM images by me and in former studies (Palomino, Burns et al. 2008) confirm the magnitude of the diameter and determine the thickness of the particles to be 50 to 100 nm. No further steps like drying were taken to alter the raw material.

Fine Illite gravels were crushed with a mortar and sieved with a 200-mesh which in theory should cap the resulting particle size to a maximum of 75 micron. The bentonite used in the study was provided by Schlumberger. It was available in the lab, but unfortunately no further information about particle or origin is available.

The Eagle Ford rock was obtained from Kocurek Industries (Cardwell, Texas, USA). They sell outcrop material retrieved from approximately 30-40 ft below surface and cut it into plugs with the intention to do triaxial tests. For the tests on powder described in this thesis offcut material remaining from the retrieved rock was sufficient. Due to the hardness of the material, grinding with pestle and mortar was not enough to gather fine material from the rock, so a ball mill (Retsch Ball Mill PM 200) was used instead (see Chapter instruments). The pre-crushed material with gravels not larger than 4mm together with 12 grinding balls were put into the grinding jars and rotated at 500min^{-1} for 5 min. After oven drying at 110°C for 4 to 6 hours the powder was sieved with a 200-mesh.

The Eagle Ford basin is a major shale play in North America known for its high carbonate content of 60 to 80% and a clay content of 20%. The interest in the shale play is partly due to the brittleness of the reservoir rock, making it very accessible with hydraulic fracturing. A high TOC up to 20% is an indication oil-wetness of the rock (Ahmed and Meehan 2016).

7.6.2 Liquids

Many concepts in this thesis deal with the interaction of fine solid material with polar and non-polar liquids. The obvious choice for the polar liquid is water, which was extensively used in deionized form as well as altered with different amounts of sodium hydroxide to increase its

pH value and hydrogen chloride to lower it. Additionally, sodium chloride and calcium chloride has been added to create brines with different salt concentrations.

Initially, general kerosene bought at a convenience store was used as the polar liquid. After a series of tests, it became evident that complete understanding of the experiments required knowledge about the exact composition of the liquid. A common method to identify organic components is by the use of a GCMS (see chapter instruments). 1µl of kerosene diluted at a ratio of 1:1000 with DCM has been injected via 1:10 split injection into the gas chromatograph using a thin capillary tube (type: HP5-MS) and heated at a rate of 5°C/min. The total ion chromatogram (see Fig. 39) reveals the complex nature of the kerosene sample. It shows major spikes for compounds consisting of 9 to 15 carbon atoms. The respective alkanes are highlighted in the plot.
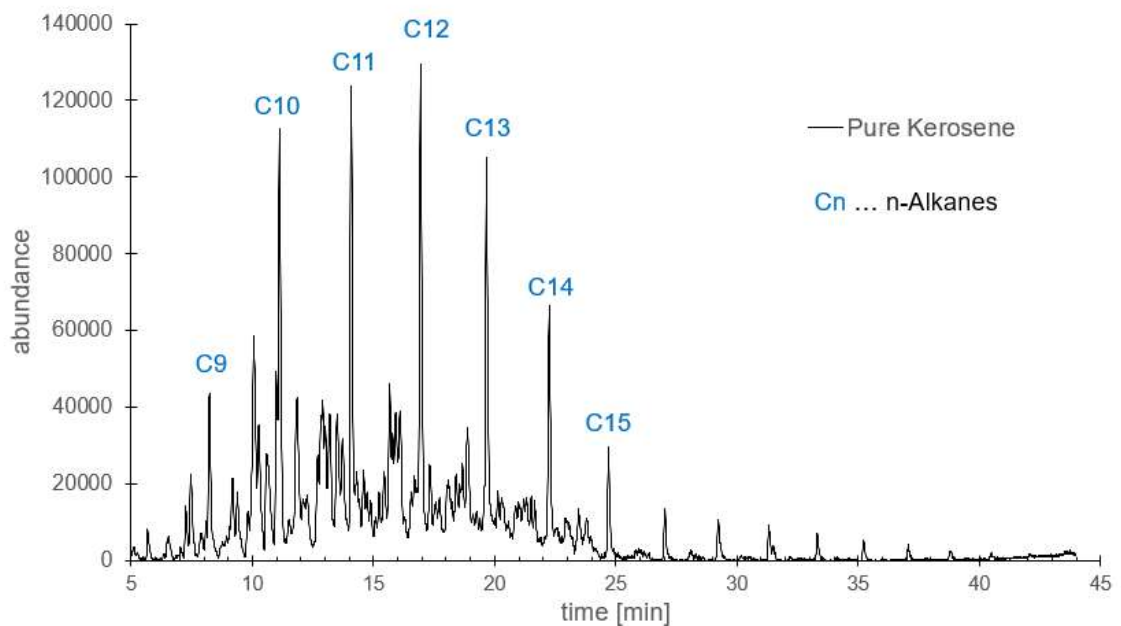

Figure 45: Total ion chromatogram from mass spectrometry measurement on kerosene

The height of the spikes can be an indication for abundance of a certain compound, but it is actually the integral of the spike or the area below it that needs to be compared to a fairly noise-free area of the whole chromatogram to get quantitative information about the composition of the sample. As an exact characterization of the kerosene seemed above the scope for the thesis literature values are used:

Table 4: Physical and chemical properties of organic liquids

	Kerosene	Decane
source	Guibet and Faure-Birchem (1999)	
Range of number of C atoms	9 to 13	10
H/C ratio	1.9-2.1	
Boiling range [°C]	140-280	174.1
Specific gravity at 15°C	0.77-0.83	0.73
Aromatics [vol%]	10-20	
Cycloalkanes [vol%]	20-30	
Paraffins [vol%]	50-65	
Rel. permittivity		1.9853 at 293.2 K

In the experiments done during the later stages of the thesis work, kerosene has been replaced by decane (Fisher Scientific, 99%, anhydrous). This step made understanding experiments and reproducibility better than with the more complicated kerosene.

7.6.3 Vials

As containments for the experiments 15ml- centrifuge tubes manufactured by VWR have been used. A lot of tests have been conducted over the course of this thesis and these vials were readily available. They are made of polypropylene, sterilized and have a conical shape at the lower part of the vial. After doing the tests described later in this thesis it became evident, that the vial favors adhesion of the oil phase. Additionally, it can be sealed with a cap, made of polyethylene.
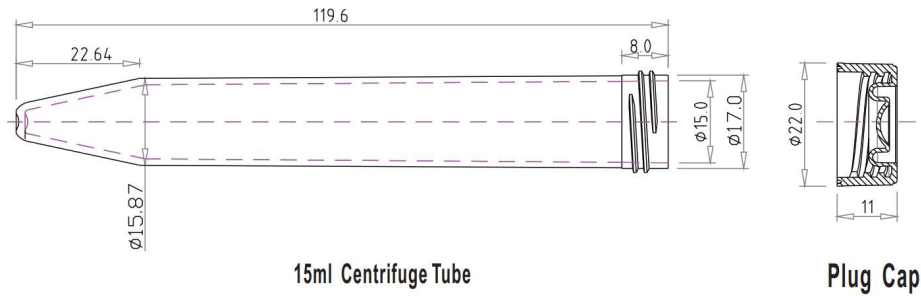
Figure 46: Dimensions of vials (from product datasheer at vwr.com)

7.7   Instruments

7.7.1   Retsch Planetary Ball Mill PM 200

The Planetary Ball Mill is a device used to pulverize course material by frictional forces. Grinding jars, filled with the chosen raw material and hard ceramic balls, sit on a sun wheel. A mechanical transmission rotates the jars in the opposite direction of the sun wheel at two times its speed. The rotational movement of the grinding balls creates friction which ultimately crush the material in the jars into fine powder. Homogeneity and particle size are controlled by the number of grinding balls used, the rotational speed and the overall processing time.

Figure 47: Retsch PM 200 (source: retsch.com)

7.7.2 Malvern Zetasizer Nano ZS

The Zetasizer Nano from Malvern used can operate in two modes, measuring particle size and zeta potential respectively. Although experiments utilizing the latter mode, where the zeta sizer measures particle speed within an applied electrical field (see electrophoresis described in chapter rock-fluid interactions) to calculate the zeta potential, were done, the device was mainly used to measure particle size. In this mode the Zetasizer measures diffusive speed of particles caused by Brownian motion. The speed of the particles is related to its size – large particles move slower than particles smaller in size. It is tracked by the Zetasizer through dynamic light scattering meaning that particles are illuminated with a laser. The reflection of the particles is observed with a photodiode at a certain angle and the scattering intensity, which changes over time depending on the speed of the particle, is correlated to the size of the particle.

7.7.3 GCMS (Agilent Technologies, 5975C)

Gas chromatography–mass spectrometry is an analytical method to identify certain substances within a test sample. It can be used to characterize organic components in a crude or refined oil. As the name suggests, the device consists of two main parts. The sample is vaporized in the gas chromatography and travels through a capillary tube. The components separate depending on their chemical properties and their affinity for the stationary phase of the tube and therefore elute at different so-called retention times. In the mass spectrometer the components are ionized and deflected. The intensity of ions detected at certain deflection strengths are used to determine mass to charge ratios m/z by which compounds can be quantified. Tracking all compounds of the sample will generate a mass spectrum which can be identified when compared to a preestablished data base.
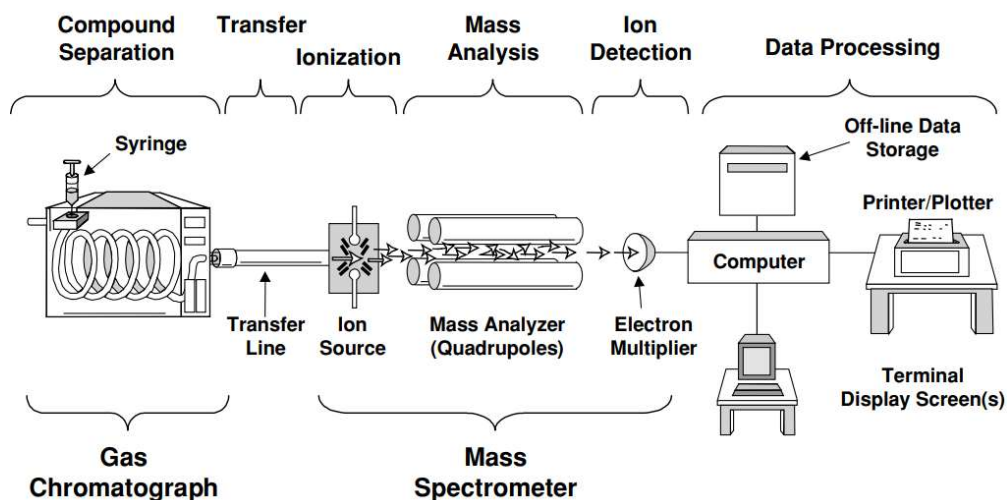

Figure 48: Components of the GCMS (Peters, Peters et al. 2005)

Generally, only a small portion of the sample is injected by the syringe to prevent overloading. It is avoided by diluting the sample for example with dichloromethane and by the use of a split-flow injector, which diverts most of the vaporized components to a vent. Splitless injection can be used if very small quantities have to be detected for example to analyze biomarkers used in the petroleum industry.

To illustrate the characterization process I used toluene, an aromatic hydrocarbon, as a test sample. The following Fig. 43 shows the resulting total ion chromatogram. A single spike shortly after starting the measurement indicates a low boiling temperature and more importantly a sample that consist solely of toluene.
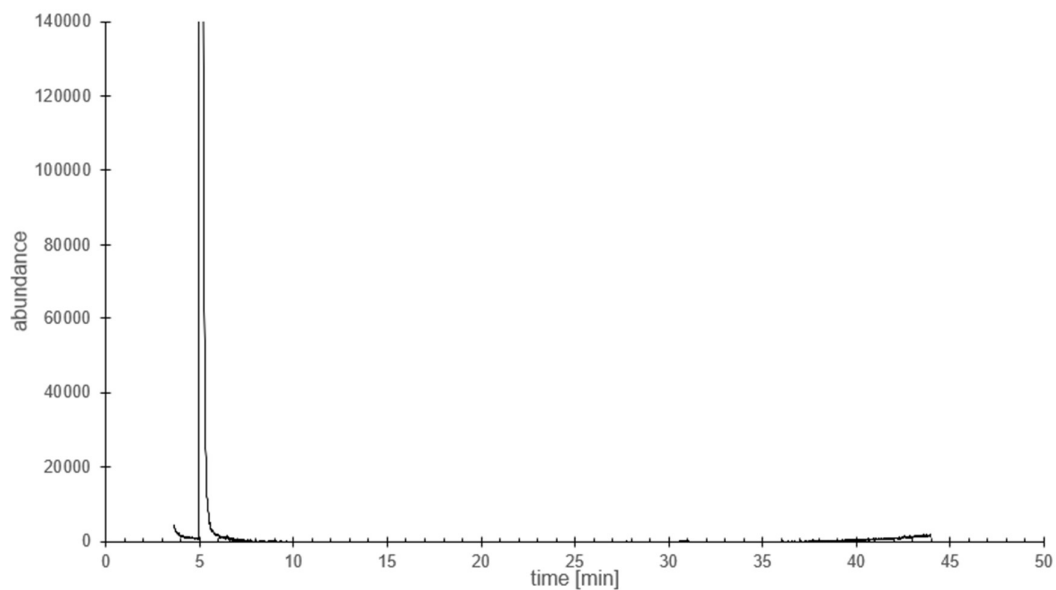

Figure 49: Total ion chromatogram for toluene

The spike is analyzed by calculating the average mass spectrum during the occurrence of the spike (Fig. 44 left) and comparing it with reference spectra in a data base. In this case a 95.9%-match with toluene confirms the nature of the sample.
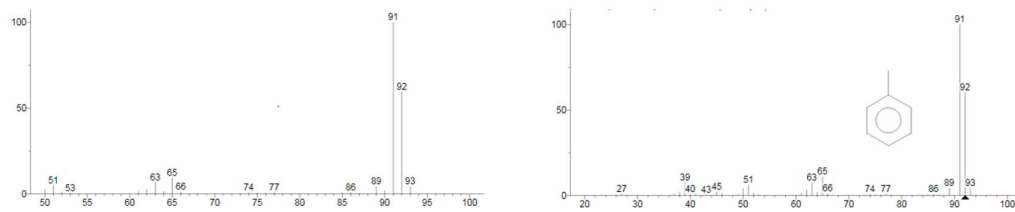

Figure 50: (left): Average Ion Chromatograph from 4.963min to 5.279min, (right): reference spectrum of toluene

7.7.4 Image capturing

A Sony ILCE-5000 has been used for image capturing, video capturing and time lapse photography. Sony provides a software suite called Imaging Edge, that allows to control the camera from a computer and save the images and videos directly to the hard drive, which helps to avoid storage capacity issues for example during over-night time-lapse photography experiments.

The image processing was done in Adobe Premiere 2018.

7.7.5 Microscope Leica DMS 300

The Leica DMS 300 is digital microscope system, that can be connected to a monitor and controlled via computer. In this case, the matching off scale and image capturing was done via the Leica Application Suite (v4.6.2). The main object magnification used was 0.8.